# Resource Competition Shapes the Response of Genetic Circuits

Yili Qian[1†], Hsin-Ho Huang[1†], José I. Jiménez[1,2], Domitilla Del Vecchio[1,3,*]

[1] Department of Mechanical Engineering, Massachusetts Institute of Technology, Cambridge, MA, USA
[2] Faculty of Health of Medical Sciences, University of Surrey, Guildford, UK
[3] Synthetic Biology Center, Massachusetts Institute of Technology, Cambridge, MA, USA
[†] These authors contributed equally to this work.
∗ Correspondence: ddv@mit.edu

## Supporting Information

Part A of the SI contains a detailed description of the experimental methods, materials and additional data. Part B contains derivation and analysis of the mathematical models.

## Part A

## A1 Constructions of activation cascades

The CAS-1 plasmid (see Figure S1) was constructed using the vector J86001 [1] as a scaffold in a three-step process using isothermal assemble [2]. First, the constitutive promoter of the GFP module in J86001 was replaced by the *sal* promoter. This was achieved by the successive addition of the core region of the promoter by PCR amplifying J86001 with oligonucletides Psal5 and Psal3 ,and the operator regions of the promoter amplifying the product of the previous PCR with complementary oligonucleotides Psal2_5 and Psal2_3 to render pPSalC. In a second step, the *rfp* gene in pPSalC was replaced by the *nahR* gene. Both fragments, the plasmid scaffold using the template pPSalC and oligonucleotides J87001_2_5 and J87001_2_3 and the insert nahR using the BioBrick Part BBa_K598026 as a template and oligonucleotides NahR5/NahR3 were assembled as the vector J87001. Third, the origin of replication of J87001 was replaced with the ColE2 origin, resulting in the CAS-1 plasmid: the ColE2 origin was amplified from the plasmid pFM371 (gift from Felix Moser, MIT) with oligonucleotides ColE2_5/ColE2_3, and the J87001 was amplified with oligonucleotides J88001_5 and J88001_3. The CAS-0.3 plasmid was obtained after PCR amplification of CAS-1 plasmid with the overlapping oligonucleotides J93032-5 and J93032-3 designed to replace the ribosome binding site (RBS) BBa_B0034 of *nahR* gene with a weaker variant BBa_B0032. To tune the copy number of a plasmid, the CAS-1 and CAS-0.3 plasmids were transformed into *E. coli* DIAL JTK160 J and H strains to create the four activation cascades CAS 1/60, CAS 1/30, CAS 0.3/60, and CAS 0.3/30. A ColE2 plasmid in the DIAL J and H strains has around 60 and 30 copies, respectively, in exponential growth [3].

Primers for cloning an activation cascade were listed in FASTA format as followed.

>Psal5
ccgttatcgttattaacaagtcatcaataaagccatcacgagtaccatagtactagagaaagaggagaaatactagatgcgtaaaggaga
>Psal3
ctttattgatgacttgttaataacgataacggagcaaacaatattgataaatactctagtatggtgcaaaacctttcgcggtatggcatg
>Psal2_5
ccgggcgcaatattcatgttgatgatttattatatatcgagtggtgtatttatcaatattgtttgctccgttatcgttattaacaagtc
>Psal2_3
caccactcgatatataataaatcatcaacatgaatattgcgcccggctctagtatggtgcaaaacctttcgcggtatggcatgatagcg

>J87001_2_5
ctagtatttctcctctttctctagtatttattcgactataacaaaccattttcttgcgtaaacctgtacgatcctacaggtctctag
>J87001_2_3
cgctgatagtgctagtgtagatcgctactagagtactagctctagatgcggccgcgaattcc
>NahR_5
gaaaatggtttgttatagtcgaataaatactagagaaagaggagaaatactagatggaactgcgtgacctggatttaaacctgctggtgg
>NahR_3
agctagtactctagtagcgatctacactagcactatcagcgtcaatccgtaaacaggtcaaacatcagttgccgca
>ColE2_5
ggccagcaaaaggccaggaaccgtaaaaaggccgccctcgaggagcgcctcagcgcgccgtagcgtcg
>ColE2_3
ccactgagcgtcagaccccgtagaaaagagggcccgagcttaagactggccgtcgttttacacctagg
>J88001_5
tcttttctacggggtctgacgctcagtgg
>J88001_3
cggccttttttacggttcctggccttttgc
>J93032-5
ctagagtcacacaggaaagtactagatggaactgcgtgacctggatttaaacctgctgg
>J93032-3
ctagtactttcctgtgtgactctagtatttattcgactataacaaaccattttcttgcg

## A2 Bacterial cells cultivation

The 15 % glycerol stock of the bacterium *E coli* DIAL strain cells stored at −80 °C were streaked on a LB (Luria-Bertani) agar plate containing 100 µg mL$^{-1}$ ampicillin and 50 µg mL$^{-1}$ kanamycin and incubated at 37 °C for 16 hours. A single colony was inoculated in a 1 mL growth medium with the respective antibiotics in a well of a 24-well plate (Falcon, no. 351147) and incubated at 30 °C, 200 rpm for 9 hours to reach OD value at 600 nm about 0.3. The growth medium is the minimal M9 medium supplemented with 4 g L$^{-1}$ glucose, 2 g L$^{-1}$ casamino acids, and 1 mM thiamine hydrochloride. The culture was then diluted 400-fold in the growth medium containing the respective antibiotics and a inducer salicylate (SAL) 1 mM and distributed 1 mL per well in a 24-well plate. The plate was incubated at 30 °C, 200 rpm for 2-3 hours to enter early exponential phase of the growth and then each well was induced by another inducer *N*-hexanoyl-L-homoserine lactone (AHL) at the indicated concentration. There were twenty-four AHL concentrations as 0, 0.03, 0.05, 0.08, 0.10, 0.20, 0.40, 0.80, 1.00, 1.95, 3.91, 7.81, 12.5, 15.6, 25.0, 31.3, 50.0, 62.5, 100, 125, 200, 250, 500, and 1000 nM.

## A3 Flow cytometry and growth rate estimation

Each culture was sampled 10 µL h$^{-1}$ and replenished the same volume of the fresh growth medium containing the respective inducers and antibiotics. GFP expression in a single cell was quantified by the flow cytometer Accuri C6 (BD). The parameters were the threshold 7000 on FSC-H, the flow rate 66 µL min$^{-1}$, the core size 13 µm, and a proper gating on FSC-H and SSC-H to exclude the background and gate the target the cell population. The sampled culture was kept on ice and was diluted right before running cytometry with 0.22 µm-filtrated water to make the reading rate is about 1000 events per second. Total collected events were 50000. GFP intensity was analyzed with the BD Accuri C6 software to obtain the arithmetic mean of a population. Growth rate was estimated from the gated data in events per µL by the flow cytometer.

## A4 Growth of activation cascade constructs

The activation cascade constructs CAS 1/60, CAS 1/30, CAS 0.3/60, and CAS 0.3/30 grew in the medium containing 1 mM SAL and the indicated concentration of AHL. The specific growth rate

during exponential growth at an indicated induced condition was shown in Figure S2. For CAS 0.3/30 and CAS 0.3/60, growth rates were consistent for all AHL levels. Due to lower plasmid copy number, CAS 0.3/30 induced lower metabolic burden on the host cell. Consequently, its growth rate was higher then those of CAS 0.3/60.Growth rates of CAS 1/60 and CAS 1/30 changed with AHL inputs. For low AHL input (less than 10 nM) levels, growth rates were roughly unchanged. For higher AHL input levels, host cell growth rate decreased. This is especially significant for CAS 1/60, in which we observed more than 90% decrease in growth rate. These phenomena are consistent with previous experimental results and theoretical study [4, 5, 6, 7, 8, 9], where it was shown that increase in synthetic circuit resource demand may overload the host cells, reducing their growth rate.

Notice that slower growth rates of the host cells can not solely explain monotonically decreasing (or biphasic) dose response curves of the activation cascade we observed in Figure 3. Two pieces of evidence supports this reasoning. First, a similar trend of gradually reduced growth rates were observed at a higher titer beyond a certain induction level in CAS 1/30 and CAS 1/60 in the induced conditions of a constant SAL (1 mM) and titrating AHL (Figure S6), and a constant AHL (100 nM) and titrating SAL (Figure S8). However, GFP concentration decreased with AHL in the presence of a constant SAL (Figure 3) while it increased with SAL in the presence of a constant AHL (Figure S7).

Therefore, the decrease in green fluorescent protein (GFP) concentration in the activation cascade CAS 1/60 and CAS 1/30 is not necessarily a consequence of slower cell growth rates. Furthermore, the only difference between the control experiment setup (Figure 1B) and the activation cascade setup (Figure 1C) is that NahR production was inducible in the activation cascade, while constitutive in the control experiment. Therefore, decrease in GFP is most likely to be caused by simultaneous increase in production of GFP and NahR, rather than the fact that both are existent in cells in large amounts.

Our second piece of evidence to rule out slower cell growth leading to decreased GFP amount is a previous research on circuit-host interactions [8]. According to the mathematical model and experimental results in [8], for an activated gene, slower growth rate leads to increases in its concentrations. These results take into account both change in dilution rate and the availability of total resources as a consequence of slower host cell growth. Considering the activation cascade, were there no competition between NahR and GFP for cellular resources, but only competition between the synthetic circuit as a whole and the endogenous circuit of the host cell, lower cell growth rate would lead to an increase in NahR concentration, further promoting the production of GFP, whose concentration itself would have increased already with slower growth rate. However, our experimental results in Figure 3 contradicted this hypothesis. Therefore, the decrease in GFP concentration we observed in the activation cascade could not be explained by decrease in cell growth rate alone. Factors other than host-circuit interaction must be included to explain the negative or biphasic dose response of an activation cascade.

## A5 Step-wise dose response curve of transcriptional activation by NahR

To access the transcription activation by NahR at the second stage of the genetic cascade CAS 1/30, we added 100 nM AHL to constitutively express NahR proteins and titrated NahR's ligand SAL from 0 to 5000 µM to acquire the dose response curve of NahR. We observed a two-step monotonic increasing dose response curve. The Hill coefficients were around 2 for both induction steps by NahR in CAS 1/30 (Figure S3a). Similarly, this two-step monotonic increasing curve was also observed for the CAS 1/60, but the Hill coefficients were around 2 and 8, respectively, for the induction at lower and higher titer (Figure S3b). To illustrate the functionality of the second stage of CAS 1/30 in Figure 1b, we only showed the titration curve of NahR activation up to 100 µM SAL to focus on its monotonic response in an induction step.

It has been evidenced that NahR without chelating its ligand SAL readily binds the $P_{sal}$ promoter and that prebound NahR requires SAL to promote transcriptional activation [10]. From Surface Plasmon Resonance (SPR) analysis [11], in the absence of SAL, NahR bound to the $P_{sal}$ promoter in a ratio from 1:1 to 8:1 when NahR concentration increased. Based on these evidences, we suspected

4 and 10 prebound NahR proteins on the $P_{sal}$ promoter of CAS 1/30 and CAS 1/60, respectively, deducing from the sum of Hill coefficients of the induction steps at a lower and a higher titer (i.e. 2+2 and 2+8). The inferred number of the prebound NahR proteins is proportion to a low and high constitutive expression level of NahR in CAS 1/30 and CAS 1/60 under 100 nM AHL induction due to a low and high plasmid copy number, respectively. We used 1000 µM SAL to fully activate transcription by the prebound NahR on the $P_{sal}$ promoter in CAS 1/60 (Figure S3b). The same concentration was also used in other three activation cascades because cell culture showed a reduced growth rate when treated with more than 1000 µM SAL.

In Figure 4, when the input AHL was higher than 10 nM to express more NahR, NahR pre-bound to the $P_{sal}$ promoter in a multimer form and in the presence of 1000 µM SAL, the NahR·DNA complex achieve a higher transcription activation. Due to different RBS strength and plasmid copy number, a higher transcription activation by NahR started slightly different at 1.95 nM, 7.81 nM, 10.0 nM, and 12.5 nM AHL for CAS 1/60, CAS 1/30, CAS 0.3/60, and CAS 0.3/30, respectively, deducing from the output GFP level. Under resource competition, even though a higher activation was achievable by NahR, CAS 1/60 showed a local increase of GFP output but still showed a negative response after 10 nM AHL. Similarly, for CAS 1/30, we observed a local increase of GFP output around 10 nM AHL on the right-hand side of a biphasic curve; for CAS 0.3/60, a local increase of GFP output around 10 nM AHL merged with the turning section of a biphasic curve; for CAS 0.3/30 which had least resource competition between *nahR* and *gfp* gene expressions, a higher activation by NahR leaded to a higher GFP output level.

## A6 Detailed experimental data

Dose response curves in Figure 1A-B and Figure 4 without normalization are presented in Figure S5, Figure S3A (when SAL concentration is between 0.01 and 100 µM as described in Section A5), and Figure S6, respectively.

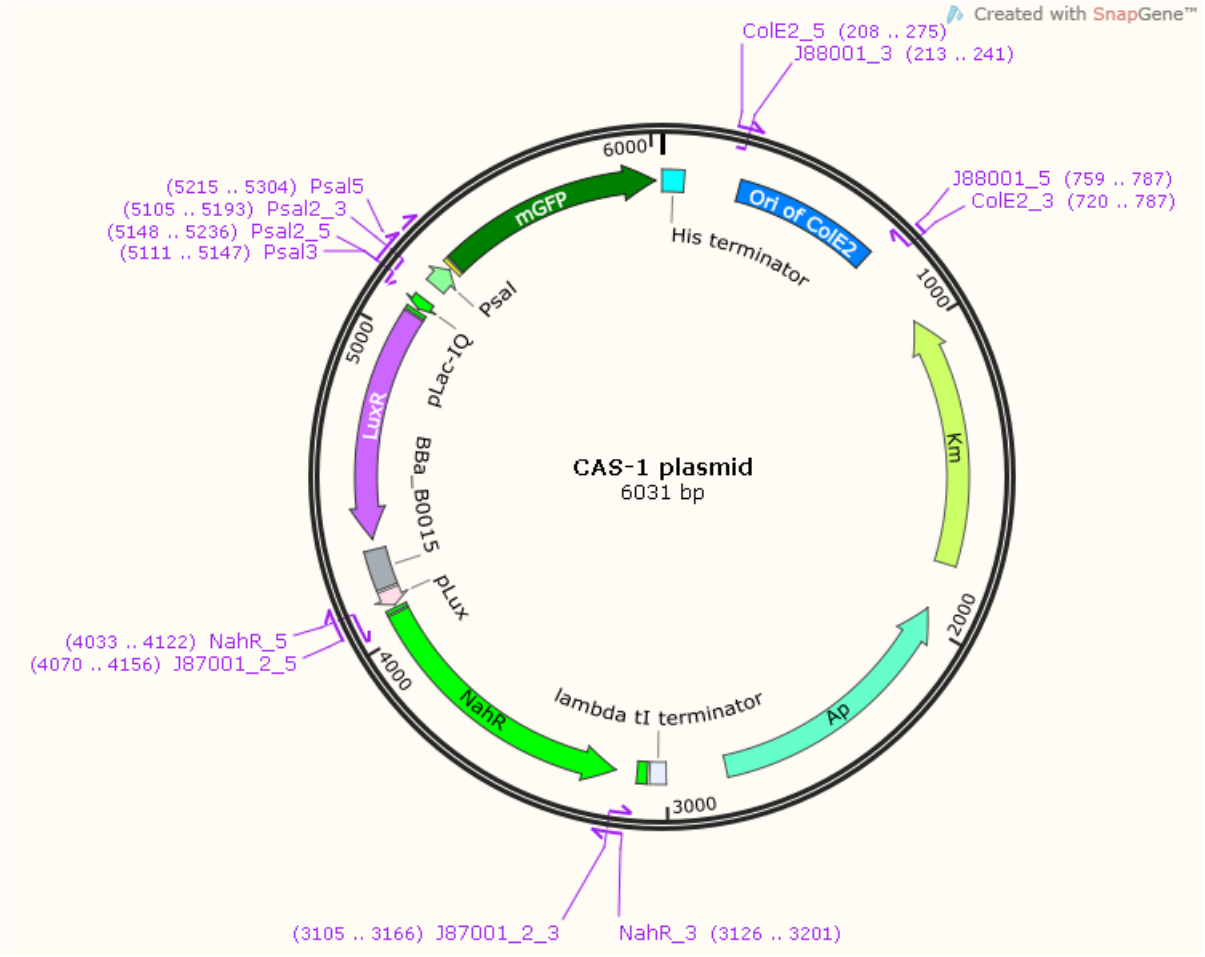


Figure S1: The plasmid map of CAS-1.

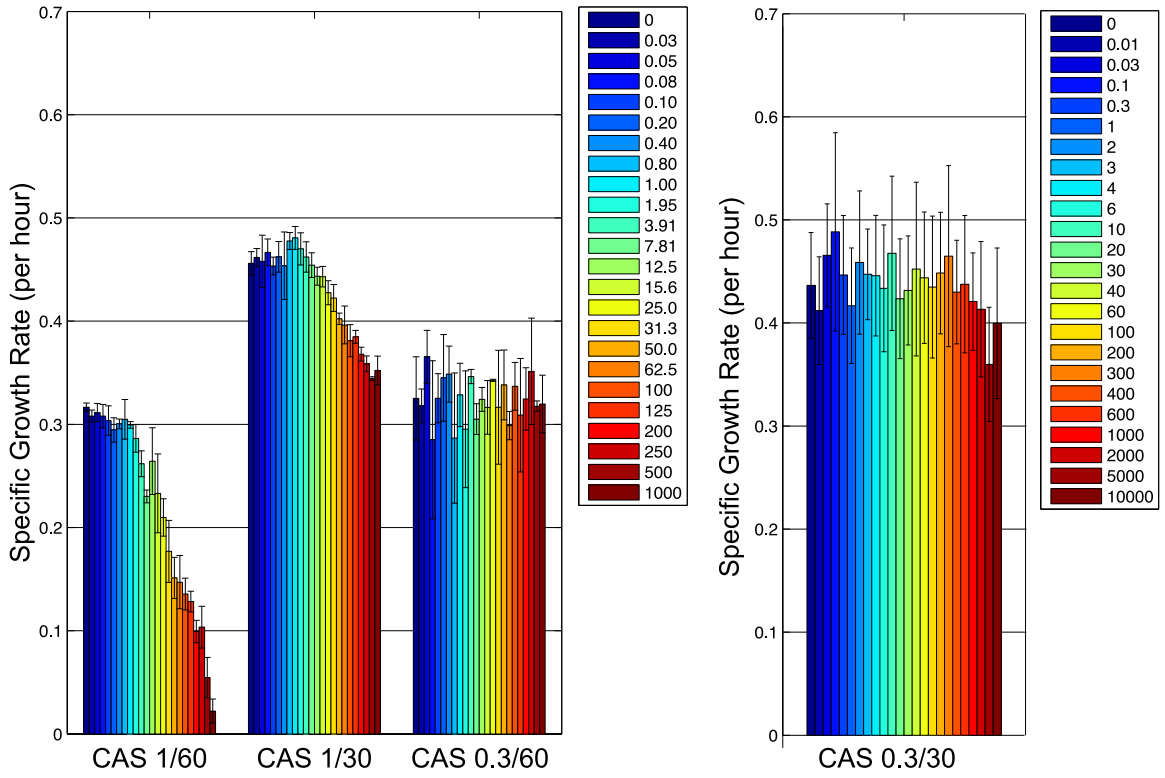


Figure S2: Exponential growth of the four activation cascades induced by adding 1 mM SAL and the indicated AHL concentration. The mean and the standard deviation of specific growth rates during exponential growth measured in three independent experiments at the indicated AHL concentration (nM) were presented by a bar with an error bar.

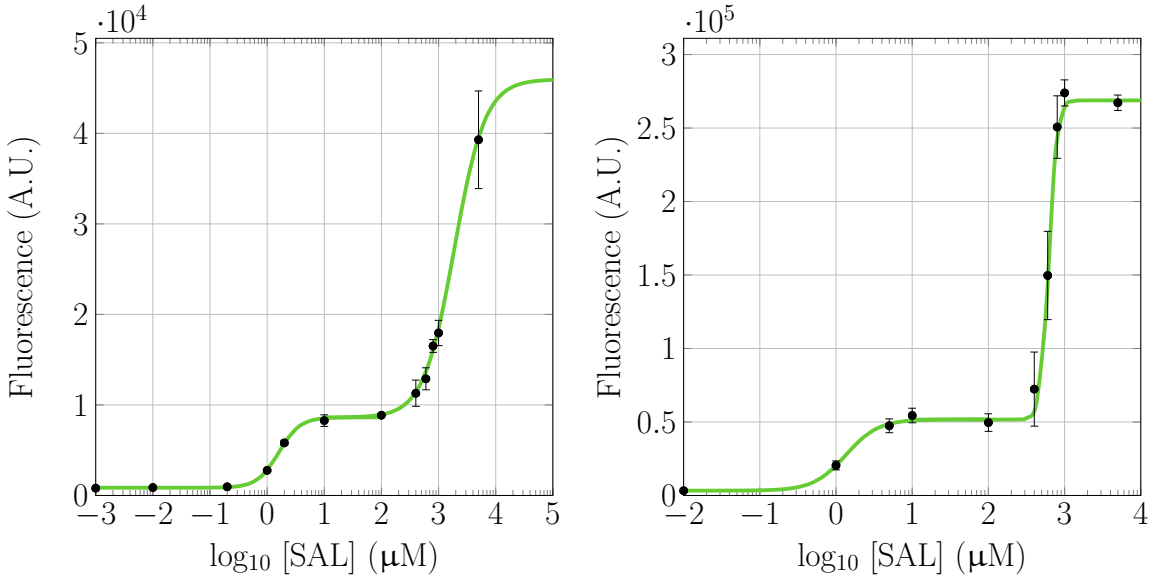


Figure S3: Dose response curves of the two activation cascades (a) CAS 1/30 and (b) CAS 1/60 under the inductions of 100 nM AHL and the indicated concentration of SAL.

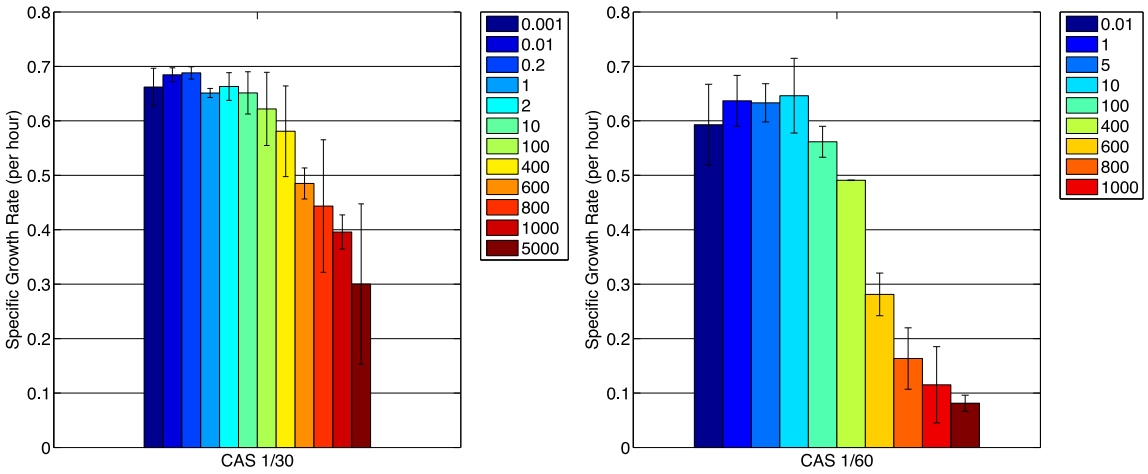


(a) (b)

Figure S4: Exponential growth rates of the two activation cascades (a) CAS 1/30 and (b) CAS 1/60 under the inductions of 100 nM AHL and the indicated concentration of SAL.

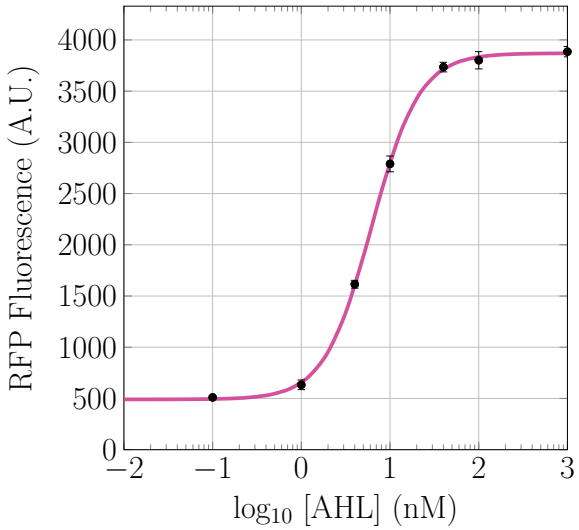


Figure S5: The dose response curve in Figure 1A without normalization.

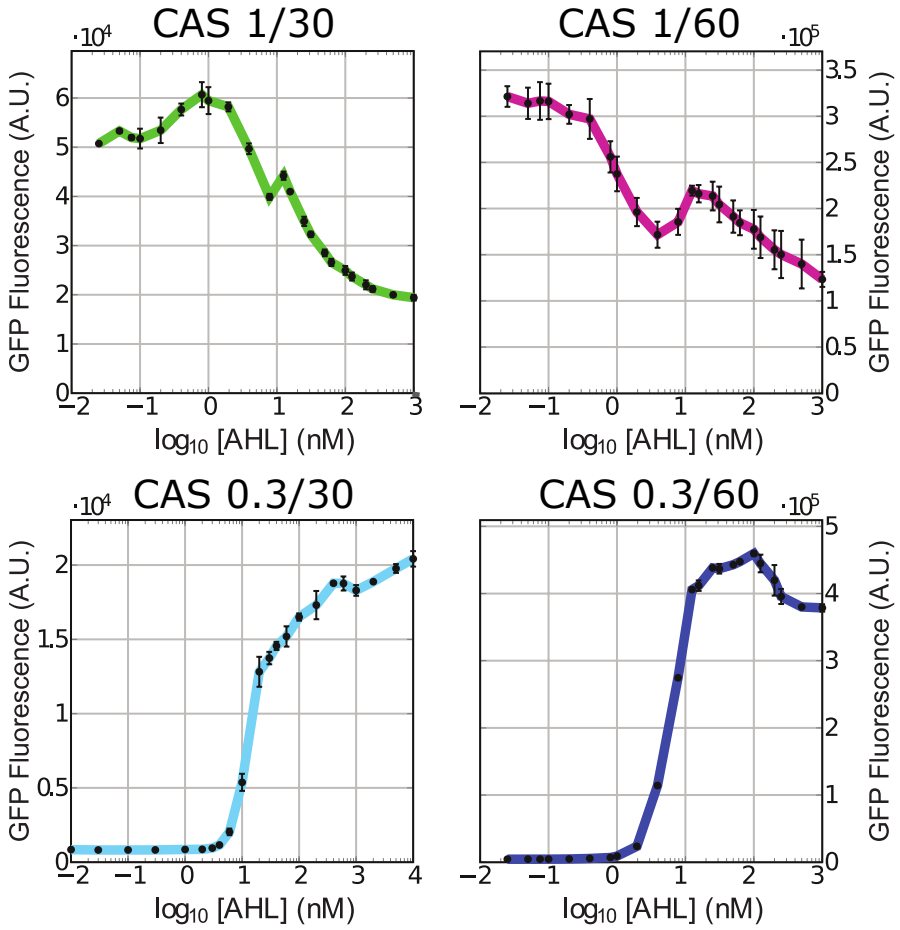


Figure S6: The dose response curves of Figure 4 without normalization.

# Part B

## B1 Derivation of a standard activation cascade model

A two-stage activation cascade is consists of a TF+effector complex u that activates node 1 to produce $x_1$, which further serve as a TF input that activates node 2 to produce protein $x_2$. This activation cascade can be view as an input/output system that takes $u$ (concentration of u) as input, and produce $x_2$ (concentration of $x_2$) as output. Here, we derive the standard Hill function model to describe the dose response (steady state input/output response) of this circuit.

In node 1, the input TF (u) binds with the promoter site of gene 1 ($p_1$) to form a promoter-activator complex $c_1$, which then recruits free RNA polymerases (RNAPs) (y) to form a transcriptionally active complex $C_1$. In addition, we take into account leakiness of $p_1$ such that it can directly recruit RNAPs (but with weaker affinity) to form transcriptionally active complex $C_1^0$ without the help of u. Letting $n_1$ be the Hill coefficient capturing cooperativity of u binding with $p_1$, the chemical reactions are as follows:

$$p_1 + n_1 \cdot u \underset{k_1^-}{\overset{k_1^+}{\rightleftharpoons}} c_1, \qquad c_1 + y \underset{d_1}{\overset{a_1}{\rightleftharpoons}} C_1, \qquad p_1 + y \underset{d_1^0}{\overset{a_1^0}{\rightleftharpoons}} C_1^0.$$

The transcriptionally active complexes ($C_1$ and $C_1^0$) are then transcribed at a constant elongation rate $\alpha_1$ to produce mRNA transcripts ($m_1$), which we assume to be the same for both $C_1$ and $C_1^0$. RNAPs are released when transcription is completed. We assume mRNA transcripts are diluted during proliferation/degraded by RNase at a constant rate $\delta_1$:

$$C_1 \xrightarrow{\alpha_1} c_1 + y + m_1, \qquad C_1^0 \xrightarrow{\alpha_1} p_1 + y + m_1, \qquad m_1 \xrightarrow{\delta_1} \emptyset.$$

Translation is initiated by free ribosomes (z) binding with the RBS of mRNA $m_1$ to produce a translationally active complex $M_1$, which is then translated at a constant elongation rate $\theta_1$ to produce protein $x_1$. The protein $x_1$ (complex $M_1$) is subject to dilution due to cell growth and degradation by protease (RNase), at constant rate $\gamma_1$ ($\omega_1$). Ribosomes are released from mRNA when translation is completed, and become free again. The chemical reactions are as follows.

$$m_1 + z \underset{\kappa_1^-}{\overset{\kappa_1^+}{\rightleftharpoons}} M_1, \qquad M_1 \xrightarrow{\theta_1} m_1 + z + x_1, \qquad M_1 \xrightarrow{\omega_1} z, \qquad x_1 \xrightarrow{\gamma_1} \emptyset.$$

Chemical reactions in the second node are similar to those in the first one, except that transcription is activated by $x_1$ rather than u. Letting $n_2$ be the Hill coefficient capturing cooperativity of $x_1$ binding with promoter $p_2$, the chemical reactions are:

$$p_2 + n_2 \cdot x_1 \underset{k_2^-}{\overset{k_2^+}{\rightleftharpoons}} c_2, \quad c_2 + y \underset{d_2}{\overset{a_2}{\rightleftharpoons}} C_2, \qquad p_2 + y \underset{d_2^0}{\overset{a_2^0}{\rightleftharpoons}} C_2^0, \quad C_2 \xrightarrow{\alpha_2} c_2 + y + m_2, \quad C_2^0 \xrightarrow{\alpha_2} p_2 + y + m_2,$$

$$m_2 + z \underset{\kappa_2^-}{\overset{\kappa_2^+}{\rightleftharpoons}} M_2, \qquad M_2 \xrightarrow{\theta_2} m_2 + z + x_2, \quad m_2 \xrightarrow{\delta_2} \emptyset, \qquad M_2 \xrightarrow{\omega_2} z, \qquad x_2 \xrightarrow{\gamma_2} \emptyset.$$

Using reaction rate equations, consequently, the concentration of each species (*italic*) follows the

following ODEs:

$$\dot{c}_1 = k_1^+ p_1 u^{n_1} - k_1^- c_1 - a_1 y c_1 + d_1 C_1 + \alpha_1 C_1, \tag{S1a}$$
$$\dot{C}_1^0 = a_1^0 p_1 y - d_1^0 C_1^0 - \alpha_1 C_1^0, \tag{S1b}$$
$$\dot{C}_1 = a_1 y c_1 - d_1 C_1 - \alpha_1 C_1, \tag{S1c}$$
$$\dot{m}_1 = \alpha_1 C_1^0 + \alpha_1 C_1 - \delta_1 m_1 - \kappa_1^+ m_1 z + \kappa_1^- M_1 + \theta_1 M_1, \tag{S1d}$$
$$\dot{M}_1 = \kappa_1^+ m_1 z - \kappa_1^- M_1 - \theta_1 M_1 - \omega_1 M_1, \tag{S1e}$$
$$\dot{x}_1 = \theta_1 M_1 - \gamma_1 x_1 - n_2 k_2^+ p_2 x_1^{n_2} + n_2 k_2^- c_2, \tag{S1f}$$
$$\dot{c}_2 = k_2^+ p_2 x_1^{n_2} - k_2^- c_2 - a_2 y c_2 + d_2 C_2 + \alpha_2 C_2, \tag{S1g}$$
$$\dot{C}_2^0 = a_2^0 p_2 y - d_2^0 C_2^0 - \alpha_2 C_2^0, \tag{S1h}$$
$$\dot{C}_2 = a_2 y c_2 - d_2 C_2 - \alpha_2 C_2, \tag{S1i}$$
$$\dot{m}_2 = \alpha_2 C_2^0 + \alpha_2 C_2 - \delta_2 m_2 - \kappa_2^+ m_2 z + \kappa_2^- M_2 + \theta_2 M_2, \tag{S1j}$$
$$\dot{M}_2 = \kappa_2^+ m_2 z - \kappa_2^- M_2 - \theta_2 M_2 - \omega_2 M_2, \tag{S1k}$$
$$\dot{x}_2 = \theta_2 M_2 - \gamma_2 x_2. \tag{S1l}$$

Given that the binding reactions and mRNA dynamics are much faster than protein production and degradation [12], we can set (S1a)-(S1e), and (S1g)-(S1k) to quasi-steady state (QSS) to simplify our analysis. Since we are only interested in the dose response (steady state i/o response) of this circuit, QSS assumption does not limit the applicability and accuracy of our model. We first obtain the QSS concentrations of complexes formed with the promoters $p_1$ and $p_2$:

$$\begin{aligned} c_1 &= p_1 \left(\frac{u}{k_1}\right)^{n_1}, \quad C_1^0 = \frac{p_1 y}{K_1^0}, \quad C_1 = \frac{c_1 y}{K_1} = \frac{p_1 y}{K_1} \cdot \left(\frac{u}{k_1}\right)^{n_1}, \\ c_2 &= p_2 \left(\frac{x_1}{k_2}\right)^{n_2}, \quad C_2^0 = \frac{p_2 y}{K_2^0}, \quad C_2 = \frac{c_2 y}{K_2} = \frac{p_2 y}{K_2} \cdot \left(\frac{x_1}{k_2}\right)^{n_2}, \end{aligned} \tag{S2}$$

where we have defined the following dissociation constants:

$$k_i = \left(\frac{k_i^-}{k_i^+}\right)^{1/n_i}, \qquad K_i = \frac{d_i + \alpha_i}{a_i}, \qquad K_i^0 = \frac{d_i^0 + \alpha_i}{a_i^0} \quad (i = 1, 2). \tag{S3}$$

Dissociation constant $k_i$ describes the binding of activator u (or $x_1$) with the promoter site $p_1$ (or $p_2$), and a smaller $k_i$ indicates stronger binding. Similarly, $K_i$ and $K_i^0$ are the dissociation constants between free RNAPs and $c_1$ (or $c_2$), and between RNAPs and $p_1$ (or $p_2$), respectively. We assume activators promote recruitment of RNAPs to promoter sites, and therefore, $K_i < K_i^0$.

Let $p_{1,T}$ and $p_{2,T}$ be the total DNA copy number of the two nodes, respectively, we assume that the concentration of DNA of each node is conserved [12, 13]:

$$p_{1,T} = p_1 + c_1 + C_1 + C_1^0, \qquad p_{2,T} = p_2 + c_2 + C_2 + C_2^0. \tag{S4}$$

Using (S2) and (S4), we can find the concentrations $p_1$ and $p_2$ of the free promoters:

$$p_1 = \frac{p_{1,T}}{1 + \frac{y}{K_1^0} + (1 + \frac{y}{K_1}) \left(\frac{u}{k_1}\right)^{n_1}}, \qquad p_2 = \frac{p_{2,T}}{1 + \frac{y}{K_2^0} + (1 + \frac{y}{K_2}) \left(\frac{x_1}{k_2}\right)^{n_2}}. \tag{S5}$$

Substituting (S5) into (S2), we obtain:

$$\begin{aligned} C_1^0 &= \frac{y p_{1,T}}{K_1^0 \left[1 + \frac{y}{K_1^0} + (1 + \frac{y}{K_1}) \left(\frac{u}{k_1}\right)^{n_1}\right]}, \quad C_1 = \frac{y p_{1,T} \left(\frac{u}{k_1}\right)^{n_1}}{K_1 \left[1 + \frac{y}{K_1^0} + (1 + \frac{y}{K_1}) \left(\frac{u}{k_1}\right)^{n_1}\right]}, \\ C_2^0 &= \frac{y p_{2,T}}{K_2^0 \left[1 + \frac{y}{K_2^0} + (1 + \frac{y}{K_2}) \left(\frac{x_1}{k_2}\right)^{n_2}\right]}, \quad C_2 = \frac{y p_{2,T} \left(\frac{x_1}{k_2}\right)^{n_2}}{K_2 \left[1 + \frac{y}{K_2^0} + (1 + \frac{y}{K_2}) \left(\frac{x_2}{k_2}\right)^{n_2}\right]}, \end{aligned} \tag{S6}$$

Meanwhile, setting equations (S1d), (S1e), (S1j) and (S1k) to QSS, we obtain the following:

$$M_1 = \frac{\alpha_1 z}{\kappa_1\delta_1 + \omega_1 z}(C_1 + C_1^0), \qquad M_1 = \frac{\alpha_2 z}{\kappa_2\delta_2 + \omega_2 z}(C_2 + C_2^0), \tag{S7}$$

where we have defined $\kappa_i$ $(i = 1, 2)$ to be the effective dissociation constant of the RBS binding with free ribosomes:

$$\kappa_i = \frac{\kappa_i^- + \theta_i + \omega_i}{\kappa_i^+}, \quad (i = 1, 2). \tag{S8}$$

By incorporating into (S8) the translation rate constant $\theta_i$, and mRNA decay rate when ribosome is bound $\omega_i$, our definition of effective dissociation constant $\kappa_i$ accounts for not only the binding strength of ribosomes with RBS ($\kappa_i^-$ and $\kappa_i^+$), but also the ability of a mRNA molecule to sequester, and then occupy ribosomes. Therefore, an increase in $\kappa_i$ can either indicate weaker RBS binding with ribosomes (less ribosome recruitment), faster translation, and faster mRNA decay (both contribute to faster ribosome release). Combining equations (S7) and (S6), we therefore have

$$\begin{aligned} M_1 &= \frac{\alpha_1 z}{\kappa_1\delta_1 + \omega_1 z} \cdot \frac{yp_{1,T}}{K_1} \cdot \frac{\frac{K_1}{K_1^0} + \left(\frac{u}{k_1}\right)^{n_1}}{1 + \frac{y}{K_1^0} + \left(1 + \frac{y}{K_1}\right)\left(\frac{u}{k_1}\right)^{n_1}}, \\ M_2 &= \frac{\alpha_2 z}{\kappa_2\delta_2 + \omega_2 z} \cdot \frac{yp_{2,T}}{K_2} \cdot \frac{\frac{K_2}{K_2^0} + \left(\frac{x_1}{k_2}\right)^{n_2}}{1 + \frac{y}{K_2^0} + \left(1 + \frac{y}{K_2}\right)\left(\frac{x_1}{k_2}\right)^{n_2}}. \end{aligned} \tag{S9}$$

In a standard Hill function model, we assume that the free amount of RNAPs $y$ and that of ribosomes $z$ are constant parameters. At QSS, according to equations (S1f) and (S1l), we have

$$\begin{aligned} \dot{x}_1 &= \theta_1 M_1 - \gamma_1 x_1 = T_1 \frac{\beta_1 + \left(\frac{u}{k_1}\right)^{n_1}}{\eta_1 + \left(\frac{u}{k_1}\right)^{n_1}} - \gamma_1 x_1, \\ \dot{x}_2 &= \theta_2 M_2 - \gamma_2 x_2 = T_2 \frac{\beta_2 + \left(\frac{x_1}{k_2}\right)^{n_2}}{\eta_2 + \left(\frac{x_1}{k_2}\right)^{n_2}} - \gamma_2 x_2, \end{aligned} \tag{S10}$$

where we have defined the following lumped constants:

$$\begin{aligned} T_1 &:= \frac{\theta_1\alpha_1 p_{1,T} yz}{(\kappa_1\delta_1 + \omega_1 z)(K_1 + y)}, \quad \beta_1 := \frac{K_1}{K_1^0}, \quad \eta_1 := \frac{1 + y/K_1^0}{1 + y/K_1}, \\ T_2 &:= \frac{\theta_2\alpha_2 p_{2,T} yz}{(\kappa_2\delta_2 + \omega_2 z)(K_2 + y)}, \quad \beta_2 := \frac{K_2}{K_2^0}, \quad \eta_2 := \frac{1 + y/K_2^0}{1 + y/K_2}. \end{aligned} \tag{S11}$$

For clarity, we define Hill-functions $F_1(u)$ and $F_2(x_1)$ to characterize regulatory interactions from u to $x_1$, and from $x_1$ to $x_2$:

$$F_1(u) := \frac{\beta_1 + \left(\frac{u}{k_1}\right)^{n_1}}{\eta_1 + \left(\frac{u}{k_1}\right)^{n_1}}, \qquad F_2(x_1) := \frac{\beta_2 + \left(\frac{x_1}{k_2}\right)^{n_2}}{\eta_2 + \left(\frac{x_1}{k_2}\right)^{n_2}}. \tag{S12}$$

According to (S12), $F_1(u)$ and $F_2(u)$ are increasing Hill-functions that are normalized to 1 at their maximum. Notice that $\lim_{u\to+\infty} F_1(u) = 1$ when $u$ saturates promoters of node 1, and $F_1(0) = \beta_1/\eta_1$ is the amount of basal expression of $x_1$ relative to its maximum expression level. Similarly, $F_2(0) = \beta_2/\eta_2$, and $\lim_{x_1\to+\infty} F_2(x_1) = 1$. We consider the biologically relevant parameter region (see Section B9), where free RNAPs and ribosomes amounts are limited ($y \ll K_i, K_i^0$ and $z \ll \kappa_i$ for

$i = 1, 2$), but remains constant parameters (and therefore no resource competition in the circuit). In this case, $\eta_1, \eta_2 \approx 1$, we have

$$\begin{aligned} F_1(u) &= \frac{\beta_1 + \left(\frac{u}{k_1}\right)^{n_1}}{1 + \left(\frac{u}{k_1}\right)^{n_1}}, \quad F_2(x_1) = \frac{\beta_2 + \left(\frac{x_1}{k_2}\right)^{n_2}}{1 + \left(\frac{x_1}{k_2}\right)^{n_2}}, \\ T_1 &= \frac{\theta_1 \alpha_1 p_{1,T} yz}{K_1 \kappa_1 \delta_1}, \qquad T_2 = \frac{\theta_2 \alpha_2 p_{2,T} yz}{K_2 \kappa_2 \delta_2}. \end{aligned} \tag{S13}$$

According to (S10), the node dynamics can thus be written as:

$$\dot{x}_1 = T_1 F_1(u) - \gamma_1 x_1, \qquad \dot{x}_2 = T_2 F_2(x_1) - \gamma_2 x_2, \tag{S14}$$

which are in the same form as equations (1) in the main text. They are also consistent with standard textbook Hill function models [12, 13]. The purpose of applying the limited resource assumption $y \ll K_i, K_i^0$ and $z \ll \kappa_i$ here is to make the model (S14) comparable to the analytical model with resource competition, which is derived for this parameter region (see Section B2).

The standard model (S14) is based on the assumption that $y$ and $z$, the free amount of RNAPs and ribosomes, are constant parameters. When their availability depends on gene expression levels in the circuit, we need to explicitly write $y$ and $z$ as functions of TF concentrations, which we address in the next section.

## B2 Derivation of an activation cascade model with resource competition

Experimental evidences have suggested that the amount of RNAPs and ribosomes are key limiting factors for gene expression in bacteria with exponential growth [8, 5]. Particularly, at a constant growth rate, the total amount of RNAPs and ribosomes is conserved. In this section, instead of treating free resources as constant parameters, we use a conservation law to find an expression for the free amount of resource concentrations $y$ and $z$. For an activation cascade, RNAPs can bind with promoter-activator complex to form $C_i$ ($i = 1, 2$) or directly with the promoter to form $C_i^0$, and ribosomes can bind with the RBS site of each node to form $M_i$. These are considered as resource demand at each node, and therefore, resource conservation can be written as:

$$y_T = y + C_1 + C_1^0 + C_2 + C_2^0, \qquad z_T = z + M_1 + M_2, \tag{S15}$$

where $y_T$ and $z_T$ are the total amount of resources available to this cascade circuit, which we assume to be a constant parameter. Under the limited resource assumption, where $y \ll K_i, K_i^0$ and $z \ll \kappa_i$ ($i = 1, 2$), resources bound to the nodes can be written as:

$$\begin{aligned} C_1^0 &= \frac{yp_{1,T}}{K_1} \cdot \frac{\frac{K_1}{K_1^0}}{1 + \left(\frac{u}{k_1}\right)^{n_1}}, \quad C_1 = \frac{yp_{1,T}}{K_1} \cdot \frac{\left(\frac{u}{k_1}\right)^{n_1}}{1 + \left(\frac{u}{k_1}\right)^{n_1}}, \quad M_1 = \frac{yz\alpha_1 p_{1,T}}{\kappa_1 K_1 \delta_1} \cdot \frac{\frac{K_1}{K_1^0} + \left(\frac{u}{k_1}\right)^{n_1}}{1 + \left(\frac{u}{k_1}\right)^{n_1}}, \\ C_2^0 &= \frac{yp_{2,T}}{K_2} \cdot \frac{\frac{K_2}{K_2^0}}{1 + \left(\frac{x_1}{k_2}\right)^{n_2}}, \quad C_2 = \frac{yp_{2,T}}{K_2} \cdot \frac{\left(\frac{x_1}{k_2}\right)^{n_2}}{1 + \left(\frac{x_1}{k_2}\right)^{n_2}}, \quad M_2 = \frac{yz\alpha_2 p_{2,T}}{\kappa_2 K_2 \delta_2} \cdot \frac{\frac{K_2}{K_2^0} + \left(\frac{x_1}{k_2}\right)^{n_2}}{1 + \left(\frac{x_1}{k_2}\right)^{n_2}}. \end{aligned} \tag{S16}$$

Substituting equations (S16) into (S15), the free amount of resources can be found to be:

$$\begin{aligned} y &= \frac{y_T}{1 + \frac{p_{1,T}}{K_1}\left[\frac{\frac{K_1}{K_1^0} + \left(\frac{u}{k_1}\right)^{n_1}}{1 + \left(\frac{u}{k_1}\right)^{n_1}}\right] + \frac{p_{2,T}}{K_2}\left[\frac{\frac{K_2}{K_2^0} + \left(\frac{x_1}{k_2}\right)^{n_2}}{1 + \left(\frac{x_1}{k_2}\right)^{n_2}}\right]}, \\ z &= \frac{z_T}{1 + \frac{\alpha_1 p_{1,T}}{\kappa_1 K_1 \delta_1} y\left[\frac{\frac{K_1}{K_1^0} + \left(\frac{u}{k_1}\right)^{n_1}}{1 + \left(\frac{u}{k_1}\right)^{n_1}}\right] + \frac{\alpha_2 p_{2,T}}{\kappa_2 K_2 \delta_2} y\left[\frac{\frac{K_2}{K_2^0} + \left(\frac{x_1}{k_2}\right)^{n_2}}{1 + \left(\frac{x_1}{k_2}\right)^{n_2}}\right]}. \end{aligned} \tag{S17}$$

From (S17), we find

$$y \cdot z = \frac{y_T z_T}{1 + \frac{p_{1,T}}{K_1}\left(1 + \frac{\alpha_1 y_T}{\kappa_1 \delta_1}\right)\left[\frac{\frac{K_1}{K_1^0} + \left(\frac{u}{k_1}\right)^{n_1}}{1 + \left(\frac{u}{k_1}\right)^{n_1}}\right] + \frac{p_{2,T}}{K_2}\left(1 + \frac{\alpha_2 y_T}{\kappa_2 \delta_2}\right)\left[\frac{\frac{K_2}{K_2^0} + \left(\frac{x_1}{k_2}\right)^{n_2}}{1 + \left(\frac{x_1}{k_2}\right)^{n_2}}\right]}. \tag{S18}$$

To simplify notations, for $i = 1, 2$, we let

$$J_i := \frac{p_{i,T}}{K_i}\left(1 + \frac{\alpha_i y_T}{\kappa_i \delta_i}\right). \tag{S19}$$

Recall that $K_i/K_i^0 = \beta_i$, using (S19) and Hill-functions defined in (S13), equation (S18) becomes:

$$y \cdot z = \frac{y_T z_T}{1 + J_1 F_1(u) + J_2 F_2(x_1)}. \tag{S20}$$

Meanwhile, at QSS, according to equations (S1f) and (S1l), we have

$$\begin{aligned} \dot{x}_1 &= \theta_1 M_1 - \gamma_1 x_1 = \frac{y z \alpha_1 \theta_1 p_{1,T}}{K_1 \kappa_1 \delta_1} \cdot \frac{\frac{K_1}{K_1^0} + \left(\frac{u}{k_1}\right)^{n_1}}{1 + \left(\frac{u}{k_1}\right)^{n_1}} - \gamma_1 x_1, \\ \dot{x_2} &= \theta_2 M_2 - \gamma_2 x_2 = \frac{y z \alpha_2 \theta_2 p_{2,T}}{\kappa_2 K_2 \delta_2} \cdot \frac{\frac{K_2}{K_2^0} + \left(\frac{x_1}{k_2}\right)^{n_2}}{1 + \left(\frac{x_1}{k_2}\right)^{n_2}} - \gamma_2 x_2, \end{aligned} \tag{S21}$$

where we have used the concentrations of $M_1$ and $M_2$ obtained from (S16). Substituting into (S21) the free amount of resources $(y \cdot z)$ in (S20), we obtain the model in (1):

$$\begin{aligned} \dot{x}_1 &= \frac{T_1 F_1(u)}{1 + J_1 F_1(u) + J_2 F_2(x_1)} - \gamma_1 x_1, \\ \dot{x}_2 &= \frac{T_2 F_2(x_1)}{1 + J_1 F_1(u) + J_2 F_2(x_1)} - \gamma_2 x_2, \end{aligned} \tag{S22}$$

with

$$T_i := \frac{y_T z_T \alpha_i \theta_i p_{i,T}}{\kappa_i K_i \delta_i}, \quad (i = 1, 2). \tag{S23}$$

Physical interpretations of the elements in model (S22) are as follows. Parameters $T_i$ are the maximum expression rate of node i. In fact, according to (S22) and (S23), an expression rate of $T_i$ can only be obtained in a fictitious scenario where all available RNAPs ($y_T$) and ribosomes ($z_T$) are engaged in the production of $\mathrm{x_i}$. The functions $F_i$ describe the extent to which a node is activated, with $F_i = 1$ indicating that node i is fully activated, and $F_i = K_i/K_i^0 = \beta_i$ when node i is expressed at its basal level. Parameter $J_i$ can be viewed as the maximum resource demand in node i. A more comprehensive discussion of $J_i$ can be found in Section B5.

## B3 Diverse dose response curves of activation cascades

In this section, we use our model (S22) to thoroughly study the dose response curve of a two-stage activation cascade. By investigating the slope of its dose response curve as a function of the input concentration, we show that an activation cascade can exhibit various shapes of dose response curves, including monotonically increasing, monotonically decreasing and biphasic. By engineering biologically relevant parameters, such as DNA copy numbers, RBS strengths, and promoter leakiness, all three shapes of the dose response curves can be obtained.

## B3.1 Slope of the dose response curve of an activation cascade

The dose response curve of an activation cascade can be derived by solving for the steady state in (S22) for various $u$ values. Due to the nonlinearity and complexity of the network, analytical expression of the steady state is hard to obtained. In order to investigate the dose response curve without solving it explicitly, we take a differential perspective, which allows us to identify the sign of the slope of the dose response curve for various inputs and parameter conditions. This mathematical tool is stated in the following claim.

**Claim 1.** Consider a monostable time-invariant single-input-single-output (SISO) system:

$$\dot{\mathbf{x}} = f(\mathbf{x}, u), \qquad\qquad y = g(\mathbf{x}, u),$$

where $f(\mathbf{x}, u)$ and $g(\mathbf{x}, u)$ are analytic functions with respect to their arguments. Let the linearized system at input $\bar{u}$ and corresponding locally asymptotically stable equilibrium $\bar{\mathbf{x}}$ be

$$\dot{\tilde{\mathbf{x}}} = A\tilde{\mathbf{x}} + B\tilde{u}, \qquad\qquad \tilde{y} = C\tilde{\mathbf{x}} + D\tilde{u}.$$

Let the steady state i/o response (dose response) of the nonlinear system be $\bar{y} = \mathcal{G}(\bar{u})$, then the slope of the dose response curve at $(\bar{\mathbf{x}}, \bar{u})$ can be found by the DC gain of the linearized system, that is,

$$\left.\frac{\mathrm{d}\bar{y}}{\mathrm{d}u}\right|_{\bar{\mathbf{x}},\bar{u}} = H(0) = -CA^{-1}B + D. \tag{S24}$$

*Proof.* In the linearized model, $A = \frac{\partial f}{\partial \mathbf{x}}|_{\bar{\mathbf{x}},\bar{u}}$, $B = \frac{\partial f}{\partial u}|_{\bar{\mathbf{x}},\bar{u}}$, $C = \frac{\partial g}{\partial \mathbf{x}}|_{\bar{\mathbf{x}},\bar{u}}$ and $D = \frac{\partial g}{\partial u}|_{\bar{\mathbf{x}},\bar{u}}$. Therefore,

$$\left.\frac{\mathrm{d}\bar{y}}{\mathrm{d}u}\right|_{\bar{\mathbf{x}},\bar{u}} = \underbrace{\frac{\partial g(\bar{\mathbf{x}}, \bar{u})}{\partial \mathbf{x}}}_{C} \cdot \frac{\mathrm{d}\bar{\mathbf{x}}}{\mathrm{d}u} + \underbrace{\frac{\partial g(\bar{\mathbf{x}}, \bar{u})}{\partial u}}_{D}. \tag{S25}$$

Since $\bar{\mathbf{x}}$ satisfies $f(\bar{\mathbf{x}}, \bar{u}) = 0$, using the implicit function theorem, we have,

$$\frac{\mathrm{d}\bar{\mathbf{x}}}{\mathrm{d}u} = -\underbrace{\left[\frac{\partial f(\bar{\mathbf{x}}, \bar{u})}{\partial \mathbf{x}}\right]^{-1}}_{A^{-1}} \cdot \underbrace{\frac{\partial f(\bar{\mathbf{x}}, \bar{u})}{\partial u}}_{B} = -A^{-1}B. \tag{S26}$$

Matrix $A$ is invertible because the equilibrium $\bar{\mathbf{x}}$ is asymptotically stable. Combining equations (S25) and (S26), we obtain $\left.\frac{\mathrm{d}\bar{y}}{\mathrm{d}u}\right|_{\bar{\mathbf{x}},\bar{u}} = H = -CA^{-1}B + D$. □

Applying Claim 1 to the two-stage activation cascade model (S22), re-written here as

$$\dot{x}_1 = G_1(u, x_1) - \gamma_1 x_1, \qquad\qquad \dot{x}_2 = G_2(u, x_1) - \gamma_2 x_2, \tag{S27}$$

where we have defined

$$G_1(u, x_1) := \frac{T_1 F_1(u)}{1 + J_1 F_1(u) + J_2 F_2(x_1)}, \qquad G_2(u, x_1) := \frac{T_2 F_2(x_1)}{1 + J_1 F_1(u) + J_2 F_2(x_1)}, \tag{S28}$$

as the rate of expression of $\mathrm{x}_1$ and $\mathrm{x}_2$. We linearize (S27) at an input $\bar{u}$ and equilibrium $\bar{\mathbf{x}}$ to obtain:

$$A = \begin{bmatrix} \frac{\partial G_1}{\partial x_1} - \gamma_1 & 0 \\ \frac{\partial G_2}{\partial x_1} & -\gamma_2 \end{bmatrix}, \qquad B = \begin{bmatrix} \frac{\partial G_1}{\partial u} \\ \frac{\partial G_2}{\partial u} \end{bmatrix}, \qquad C = \begin{bmatrix} 0 & 1 \end{bmatrix}, \qquad D = 0. \tag{S29}$$

Substituting (S29) into (S24) in Claim 1, we obtain:

$$\frac{\mathrm{d}\bar{x}_2}{\mathrm{d}u} = H(0) = \frac{\frac{\partial G_2}{\partial x_1} \cdot \frac{\partial G_1}{\partial u} + \left(\gamma_1 - \frac{\partial G_1}{\partial x_1}\right) \cdot \frac{\partial G_2}{\partial u}}{\left(\gamma_1 - \frac{\partial G_1}{\partial x_1}\right) \gamma_2}, \tag{S30}$$

where $\bar{x}_2$ represent the steady state of $x_2$. Note that since we have

$$\begin{aligned}
\frac{\partial G_1}{\partial u} &= \underbrace{\frac{\partial G_1}{\partial F_1}}_{\text{positive}} \cdot \underbrace{\frac{\partial F_1}{\partial u}}_{\text{positive}} > 0, \quad \frac{\partial G_1}{\partial x_1} = \underbrace{\frac{\partial G_1}{\partial F_2}}_{\text{negative}} \cdot \underbrace{\frac{\partial F_2}{\partial x_1}}_{\text{positive}} < 0, \\
\frac{\partial G_2}{\partial u} &= \underbrace{\frac{\partial G_2}{\partial F_1}}_{\text{negative}} \cdot \underbrace{\frac{\partial F_1}{\partial u}}_{\text{positive}} < 0, \quad \frac{\partial G_2}{\partial x_1} = \underbrace{\frac{\partial G_2}{\partial F_2}}_{\text{positive}} \cdot \underbrace{\frac{\partial F_2}{\partial x_1}}_{\text{positive}} > 0.
\end{aligned} \tag{S31}$$

the denominator in (S30), $(\gamma_1 - \partial G_1/\partial x_1) > 0$, is positive. Therefore, sign$(H(0))$ depends on the sign of the numerator

$$\underbrace{\frac{\partial G_2}{\partial x_1} \cdot \frac{\partial G_1}{\partial u}}_{\text{positive}} + \underbrace{\left(\gamma_1 - \frac{\partial G_1}{\partial x_1}\right)}_{\text{positive}} \cdot \underbrace{\frac{\partial G_2}{\partial u}}_{\text{negative}} \tag{S32}$$

in (S30). According to (S31), the positivity of the numerator term in (S30) is undetermined and depends on specific parameter values. With reference to (S30), a physical interpretation of our result in is as follows. A (differential) change in $\bar{x}_2$ has two sources: the contribution from the transcriptional regulation path $\mathrm{u} \rightarrow \mathrm{x}_1 \rightarrow \mathrm{x}_2$, mathematically characterized by

$$M^+ = \left| \frac{\frac{\partial G_2}{\partial x_1} \cdot \frac{\partial G_1}{\partial u}}{\left(\gamma_1 - \frac{\partial G_1}{\partial x_1}\right)\gamma_2} \right|,$$

and a contribution from the hidden repression path due to resource competition $\mathrm{u} \dashv \mathrm{x}_2$, characterized by

$$M^- = \left| \frac{\frac{\partial G_2}{\partial u}}{\gamma_2} \right|.$$

Depending on the relative magnitude of $M^+$ and $M^-$, the slope of a dose response curve can be monotonically decreasing ($M^- > M^+$ for all $u$), monotonically increasing ($M^- < M^+$ for all $u$) or biphasic ($M^- < M^+$ for small $u$ and $M^- > M^+$ for large $u$). However, physical parameters, such as RBS strength, promoter strength and DNA copy number, are involved in $M^+$ and $M^-$ in a highly convoluted manner, and therefore, their effects on the shape of a dose response curve can hardly be singled out through (S30). In section B3.2, we consider extreme parameter relationships that allow ae dose response curve to fall into a specific class.

On the other hand, dose response curve of $\mathrm{x}_1$ is guaranteed to be monotonically increasing even in the presence of resource competition. This can be verified by applying Claim 1 to the cascade, and treating $x_1$ as its output. In this cases, we have

$$\hat{A} = A = \begin{bmatrix} \frac{\partial G_1}{\partial x_1} - \gamma_1 & 0 \\ \frac{\partial G_2}{\partial x_1} & -\gamma_2 \end{bmatrix}, \quad \hat{B} = B = \begin{bmatrix} \frac{\partial G_1}{\partial u} \\ \frac{\partial G_2}{\partial u} \end{bmatrix}, \quad \hat{C} = \begin{bmatrix} 1 & 0 \end{bmatrix}, \quad \hat{D} = D = 0. \tag{S33}$$

The static gain of the linearized system with $x_1$ as the output becomes

$$\frac{\mathrm{d}\bar{x}_1}{\mathrm{d}u} = \hat{H}(0) = \frac{\frac{\partial G_1}{\partial u}}{\gamma_1 - \frac{\partial G_1}{\partial x_1}}, \tag{S34}$$

which is guaranteed to be positive for all positive input and parameter values.

### B3.2 Sufficient parameter conditions to obtain various shapes of dose response curves

To make the dose response curve of an activation cascade to become monotonically increasing, we need to make $J_1$ sufficiently small. This can be seen from the following two perspectives. First, if

we consider the dose response of the output $x_2$, from equation (S22), we have

$$\bar{x}_2 = \frac{1}{\gamma_2} \cdot \frac{T_2 F_2(\bar{x}_1)}{1 + J_1 F_1(u) + J_2 F_2(\bar{x}_1)}. \tag{S35}$$

Notice that since $\bar{x}_1$ increases monotonically with $u$ for all input levels, and $F_2(\bar{x}_1)$ is an increasing Hill function, $F_2(\bar{x}_1)$ increases with $u$. As $J_1 \to 0$, (S35) becomes

$$\bar{x}_2 \approx \frac{1}{\gamma_2} \cdot \frac{T_2 F_2(\bar{x}_1)}{1 + J_2 F_2(\bar{x}_1)},$$

which increases monotonically with $F_2(\bar{x}_1)$, and consequently with $u$. Due to continuity, we thus expect the dose response curve to be monotonically increasing for $J_1$ sufficiently small. On the other hand, from a differential perspective, we want the slope of the dose response curve to be positive for all $u$ in order to obtain a monotonically increasing dose response curve. According to (S30) and (S32), this can be achieved if $\partial G_2/\partial u$, which represent the strength of the non-regulatory repression $u \dashv x_2$, is sufficiently small in magnitude. From (S28), we obtain

$$\frac{\partial G_2}{\partial u} = -J_1 \cdot \frac{\partial F_1}{\partial u} \cdot \frac{T_2 F_2(x_1)}{[1 + J_1 F_1(u) + J_2 F_2(x_1)]^2}.$$

Since $\lim_{J_1 \to 0} \partial G_2/\partial u = 0$, and it decreases for $J_1$ small. The slope of the dose response curve is always positive for sufficiently small $J_1$. Based on the above reasoning, here, we provide sufficient parameter conditions that guarantee the dose response curve of a two-stage cascade to be monotonically increasing, monotonically decreasing or biphasic. These results are summarized in the following claim.

**Claim 2.** If nodes 1 and 2 have the same DNA copy numbers $p_{1,T} = p_{2,T} = p_T$, and transcription rate constant $\alpha_1 = \alpha_2 = \alpha$, then in a two-stage activation cascade the slope of a dose response curve $d\bar{x}_2/du$ satisfies:

1. $\mathrm{d}\bar{x}_2/\mathrm{d}u > 0$ for all $u > 0$ if (a) $K_1 \gg p_T$ and (b) $\kappa_1 \cdot \delta_1 \gg \alpha \cdot y_T$;
2. $\mathrm{d}\bar{x}_2/\mathrm{d}u < 0$ for all $u > 0$ if (a) $p_T \gg K_2^0 > K_2 \gg K_1^0 > K_1$ and (b) $\alpha \cdot y_T \gg \delta_2 \cdot \kappa_2 \gg \delta_1 \cdot \kappa_1$;
3. $\mathrm{d}\bar{x}_2/\mathrm{d}u > 0$ when $u \to 0$ and $d\bar{x}_2/du < 0$ when $u \to \infty$ if (a) $K_1^0 \gg p_T \geq K_2 \gg K_1$ and (b) $\kappa_2 \cdot \delta_2 > \kappa_1 \cdot \delta_1 \gg \alpha \cdot y_T$.

*Proof.* Using equation (S22), the steady state concentrations of $x_1$ and $x_2$ (i.e. $\bar{x}_1$ and $\bar{x}_2$) can be written as:

$$\bar{x}_1(u, \bar{x}_1) = \frac{1}{\gamma_1} \cdot \frac{T_1 F_1(u)}{1 + J_1 F_1(u) + J_2 F_2(\bar{x}_1)}, \tag{S36}$$

$$\bar{x}_2(u, \bar{x}_1) = \frac{1}{\gamma_2} \cdot \frac{T_2 F_2(\bar{x}_1)}{1 + J_1 F_1(u) + J_2 F_2(\bar{x}_1)}. \tag{S37}$$

Note that in Section B3.1, we have shown that $\bar{x}_1$ increases monotonically with $u$, regardless of parameters. When conditions in case 1 are satisfied, we have

$$J_1 F_1(u) \leq J_1 \ll 1.$$

Equation (S37) becomes

$$\bar{x}_2(u, \bar{x}_1) \approx \frac{1}{\gamma_2} \cdot \frac{T_2 F_2(\bar{x}_1)}{1 + J_2 F_2(\bar{x}_1)}. \tag{S38}$$

From (S38), $\bar{x}_2$ increases with $\bar{x}_1$, which increases monotonically with $u$ according to (S34). Consequently, $\bar{x}_2$ is guaranteed to increase with $u$. When conditions in case 2 are satisfied, we have

$$J_1 > J_1 F_1(u) > J_1 \beta_1 \gg J_2 > J_2 F_2(\bar{x}_1) > J_2 \beta_2 \gg 1.$$

Combining with (S36), we have $\bar{x}_1 = T_1/(J_1\gamma_1) \approx$ constant, and (S37) can be viewed a single variable decreasing function of $u$. The dose response curve of the cascade is negative. When conditions in case 3 are satisfied, note that when $u \to 0$, $F_1(u) \to \beta_1$ and when $u \to \infty$, $F_1(u) \to 1$. The conditions give $J_1F_1(u) \ll 1$ when $u \to 0$, and $J_1F_1(u) \gg J_2F_2(\bar{x}_2) \gg 1$ when $u \to \infty$. The rest of the proof follows from cases 1 and 2. □

Of particular interests in Claim 2 is case 1, which enables us to restore the dose response curve of any failed cascade (with negative or biphasic dose response curves) to become positive. The parameter conditions $K_1 \gg p_T$ and $\kappa_1 \cdot \delta_1 \gg \alpha \cdot y_T$ leads to $J_1 \ll 1$, implying that node 1 has negligible maximal resource demand. These conditions can be satisfied in experiments by reducing the DNA copy number, promoter and RBS strength of node 1.

### B3.3 Practical guidance on activation cascade design

In this section, we intend to provide a more comprehensive and practical recipe on activation cascade design. In particular, we want to understand if reducing $J_1$, which allows us to obtain intended monotonically increasing dose response curve, could potentially affect some desirable feature of the circuit, such as signal amplification. Our design parameters are the RBS strengths of node 1 and node 2, and the circuit plasmid copy number, which are among the most commonly used dials in synthetic biology. Since activation cascades are often used for signal transduction and amplification, with reference to Figure S7(a), we evaluate the following performance specifications of an activation cascade:

- Shape of the dose response curve (monotonically increasing, monotonically decreasing or biphasic).
- Maximum production of output protein ($x_{2,\max}$).
- Fold activation of the cascade $x_{2,\max}/x_{2,\text{basal}}$.
- Dynamic input range, defined as the difference between input levels that achieve 90% and 10% of $x_{2,\max}$. The dynamic input range is set to be 0 if $x_{2,\text{basal}}$ is more than 10% of $x_{2,\max}$.

An ideal activation cascade should have a monotonically increasing dose response curve with large $x_{2,\max}$ and fold activation to produce detectable outputs. A large dynamic input range is ideal for applications requiring analog output to a wide range of inputs, while a small dynamic input range may be helpful to generate a "digital" (switch-like) dose response, which helps to filter noise in the form of spurious activation [14, 15]. Using the full activation cascade model (see Section B10), performances of the cascades can be visualized in Figure S7(b). We find that each performance criterion is governed by one or two key design parameters. Due to resource competition considerations, the shape of a dose response curve is determined by the RBS strengths of $x_1$ and the plasmid copy number. Meanwhile, RBS strength of $x_2$ and copy number are the dominant factors to decide $x_{2,\max}$. This is because maximum amount of $x_2$ is produced when its promoters are saturated with $x_1$. As long as a sufficient amount of $x_1$ can be produced to saturate the promoters, $x_{2,\max}$ depends solely on its own production rate, which increases with its RBS strength and copy number. Cascade fold activation decreases with plasmid copy number and $x_1$ RBS strength. To understand this result, consider the extreme case where promoters of $x_2$ are already saturated by the basal amount of $x_1$ due to its high copy number and strong RBS strength, the circuit essentially loses its activation capability. Similarly, a large dynamic input range of the cascade relies on low plasmid copy number and weak $x_1$ RBS strength.

Therefore, in order to design an activation cascade with positive dose response, large maximum output, fold activation and dynamic input range, it is advisable to use low copy plasmid with weak $x_1$ RBS strength, and strong $x_2$ RBS strength. On the contrary, to design a cascade with switch-like response, a large production rate of $x_1$ is required. This allows a large change in $x_1$ when a unit addition of $u$ is applied. Increase in $x_1$ further facilitates transition of $x_2$ from low to high. However, designing an activation cascade circuit with large $x_1$ production rate often results in negative dose response, and/or loss of activation capability, and an *ad hoc* selection of parameters may be required.

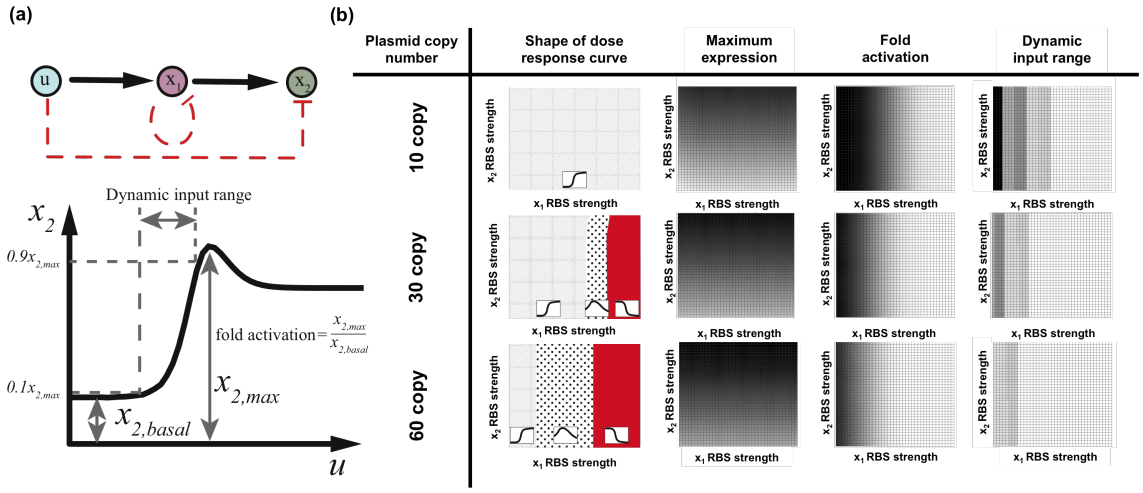


Figure S7: **Tuning the performance of an activation cascade by changing its RBS strengths and copy number.** (a) Visualization of the performance criteria used to evaluate the dose response of an activation cascade. (b) Performance of cascades with various RBS strengths and plasmid copy numbers. In each embedded figure, the horizontal axis represents the RBS strength of $x_1$, and the vertical axis represents the RBS strength of $x_2$. The three rows of embedded figures corresponds to circuits with low, medium and high DNA copy numbers. The first column of embedded figures describe the shapes of their dose response curves. The red, dotted and grid shaded region each corresponds to parameter combinations that give rise to monotonically decreasing, biphasic and monotonically increasing dose responses. The other three columns of embedded figures use gray scale to represent numerical values of maximum expression, fold activation and dynamic input range, respectively. Darker color represent large numerical values.

# B4 Model of general genetic circuits with resource limitations

The model we derived for the two-stage activation cascade in Section B1 and B2 can be extended to genetic circuits with any topology. We take a similar approach by first deriving node dynamics in isolation, treating the free amount of RNAPs and ribosomes as parameters, and then take into account sharing of these resources to decide the parameters in a network context.

## B4.1 Gene expression in a node

Since most gene promoters take at most two TF inputs [13], we consider a node i taking two input TFs ($u_i^1$ and $u_i^2$) that can either be activators or repressors, to form complexes with $p_i$. The reactions are:

$$p_i + n_i^1 \cdot u_i^1 \underset{k_{i,1}^-}{\overset{k_{i,1}^+}{\rightleftharpoons}} c_i^1, \qquad p_i + n_i^2 \cdot u_i^2 \underset{k_{i,2}^-}{\overset{k_{i,2}^+}{\rightleftharpoons}} c_i^2, \qquad c_i^1 + n_i^2 \cdot u_i^2 \underset{k_{i,12}^-}{\overset{k_{i,12}^+}{\rightleftharpoons}} c_i^{12}, \qquad c_i^2 + n_i^1 \cdot u_i^1 \underset{k_{i,21}^-}{\overset{k_{i,21}^+}{\rightleftharpoons}} c_i^{12},$$

where $n_1$ and $n_2$ are the Hill coefficients describing cooperativities of $u_i^1$ and $u_i^2$ binding with $p_i$, respectively. The promoter $p_i$ and the promoter/TF complexes ($c_i^1, c_i^2, c_i^{12}$) recruit free RNAPs (y) to form an open complex for transcription. The reactions are given by:

$$p_i + y \underset{d_i^0}{\overset{a_i^0}{\rightleftharpoons}} C_i^0, \qquad c_i^j + y \underset{d_{i,j}}{\overset{a_{i,j}}{\rightleftharpoons}} C_i^j \qquad (j = 1, 2, 12).$$

These transcriptionally active complexes can then be transcribed into mRNA ($m_i$), the reactions are given by:

$$C_i^0 \xrightarrow{\alpha_i} p_i + y + m_i, \qquad C_i^j \xrightarrow{\alpha_i} c_i^j + y + m_i, \qquad (j = 1, 2, 12).$$

Here, we assume that transcription elongation rate constant of node i ($\alpha_i$) is independent of how transcription is initiated (i.e. $\alpha_i$ is independent of the initiation complexes $\mathrm{C_i^0}, \mathrm{C_i^1}, \mathrm{C_i^2}$ and $\mathrm{C_i^{12}}$.) Translation is initiated by ribosomes (z) binding with RBS on mRNA $\mathrm{m_i}$ to form a translationally active complex $\mathrm{M_i}$, which is then translated into protein $\mathrm{x_i}$. Meanwhile, mRNAs and proteins are also diluted/degraded. The reactions are:

$$\mathrm{m_i + z} \underset{\kappa_\mathrm{i}^-}{\overset{\kappa_\mathrm{i}^+}{\rightleftharpoons}} \mathrm{M_i}, \qquad \mathrm{M_i} \xrightarrow{\theta_\mathrm{i}} \mathrm{m_i + z + x_i}, \qquad \mathrm{m_i} \xrightarrow{\delta_\mathrm{i}} \emptyset, \qquad \mathrm{M_i} \xrightarrow{\omega_\mathrm{i}} \mathrm{z}, \qquad \mathrm{x_i} \xrightarrow{\gamma_\mathrm{i}} \emptyset.$$

Consequently, we have the following ODEs in node i:

$$\dot{c}_i^j = k_{i,j}^+ p_i (u_i^j)^{n_i^j} - k_{i,j}^- c_i^j - a_{i,j} y c_i^j + d_{i,j} C_i^j + \alpha_i C_i^j, \tag{S39a}$$
$$\dot{c}_i^{12} = k_{i,12}^+ c_i^1 (u_i^2)^{n_i^2} - k_{i,12}^- c_i^{12} + k_{i,21}^+ c_i^2 (u_i^1)^{n_i^1} - k_{i,21}^- c_i^{12} - a_{i,12} c_i^{12} y - d_{i,12} C_i^{12} + \alpha_i C_i^{12}, \tag{S39b}$$
$$\dot{C}_i^0 = a_i^0 p_i y - d_i^0 C_i^0 - \alpha_i C_i^0, \tag{S39c}$$
$$\dot{C}_i^k = a_{i,k} y c_i^k - d_{i,k} C_i^k - \alpha_i C_i^k, \tag{S39d}$$
$$\dot{m}_i = \alpha_i C_i^0 + \alpha_i C_i^1 + \alpha_i C_i^2 + \alpha_i C_i^{12} - \delta_i m_i - \kappa_i^+ m_i z + \kappa_i^- M_i + \theta_i M_i, \tag{S39e}$$
$$\dot{M}_i = \kappa_i^+ m_i z - \kappa_i^- M_i - \theta_i M_i - \omega_i M_i, \tag{S39f}$$
$$\dot{x}_i = \theta_i M_i - \gamma_i x_i, \tag{S39g}$$

where indices $j = 1, 2$ and $k = 1, 2, 12$. Since DNA concentration is conserved [12], we have

$$p_{i,T} = p_i + C_i^0 + \sum_{j=1,2,12} (c_i^j + C_i^j), \tag{S40}$$

where $p_{i,T}$ is the total concentration of gene i. Assuming that binding reactions and mRNA dynamics are sufficiently fast, we obtain the QSS concentrations of complexes formed with $\mathrm{p_i}$:

$$\begin{aligned} &c_i^1 = p_i \left(\frac{u_i^1}{k_i^1}\right)^{n_i^1}, \quad c_i^2 = p_i \left(\frac{u_i^2}{k_i^2}\right)^{n_i^2}, \quad c_i^{12} = p_i \left(\frac{1}{k_i^{12}} + \frac{1}{k_i^{21}}\right) \cdot \left[\left(\frac{u_i^1}{k_i^1}\right)^{n_i^1} \cdot \left(\frac{u_i^2}{k_i^2}\right)^{n_i^2}\right], \\ &C_i^0 = \frac{p_i y}{K_i^0}, \qquad C_i^j = \frac{c_i^j y}{K_i^j}, \qquad (j = 1, 2, 12), \end{aligned} \tag{S41}$$

where dissociation constants are defined as:

$$\begin{aligned} &K_i^0 = \frac{d_i^0 + \alpha_i}{a_i^0}, \qquad K_i^j = \frac{d_{i,j} + \alpha_j}{a_{i,j}}, \qquad (j = 1, 2, 12), \\ &k_i^1 = \left(\frac{k_{i,1}^-}{k_{i,1}^+}\right)^{1/n_i^1}, \quad k_i^2 = \left(\frac{k_{i,2}^-}{k_{i,2}^+}\right)^{1/n_i^2}, \quad k_i^l = \left(\frac{k_{i,l}^-}{k_{i,l}^+}\right), \quad (l = 12, 21). \end{aligned} \tag{S42}$$

Here, $K_i^0$ is the basal dissociation constant of promoter $\mathrm{p_i}$ binding with free RNAPs y, $K_i^j$ is the dissociation constant of promoter-TF complex $\mathrm{c_i^j}$ binding with y. Parameters $k_i^1$ and $k_i^2$ are the dissociation constants of TF $\mathrm{u_i^1}$ and $\mathrm{u_i^2}$ binding with $\mathrm{p_i}$; and $k_i^{12}$ and $k_i^{21}$ are the dissociation constants of $\mathrm{c_i^1}$ binding with $\mathrm{u_i^2}$, and $\mathrm{c_i^2}$ binding with $\mathrm{u_i^1}$, respectively.

Based on (S41) and (S40), the free promoter concentration $p_i$ can be found to be

$$p_i = \frac{p_{i,T}}{1 + \frac{y}{K_i^0} + \sum_{j=1,2} \left(1 + \frac{y}{K_i^j}\right) \left(\frac{u_i^j}{k_i^j}\right)^{n_i^j} + \hat{k}_i \left(1 + \frac{y}{K_i^{12}}\right) \left(\frac{u_i^1}{k_i^1}\right)^{n_i^1} \left(\frac{u_i^2}{k_i^2}\right)^{n_i^2}}, \tag{S43}$$

where we have defined:

$$\hat{k}_i = \left(\frac{1}{k_i^{12}} + \frac{1}{k_i^{21}}\right).$$

The concentration of active open complex for node i transcription, $C_i$, is:

$$C_i = C_i^0 + \sum_{j=1,2,12} C_i^j = p_{i,T} \frac{\frac{y}{K_i^0} + \frac{y\hat{k}_i}{K_i^{12}} \left(\frac{u_i^1}{k_i^1}\right)^{n_i^1} \left(\frac{u_i^2}{k_i^2}\right)^{n_i^2} + \sum_{j=1,2} \frac{y}{K_i^j} \left(\frac{u_i^j}{k_i^j}\right)^{n_i^j}}{1 + \frac{y}{K_i^0} + \hat{k}_i \left(1 + \frac{y}{K_i^{12}}\right) \left(\frac{u_i^1}{k_i^1}\right)^{n_i^1} \left(\frac{u_i^2}{k_i^2}\right)^{n_i^2} + \sum_{j=1,2} \left(1 + \frac{y}{K_i^j}\right) \left(\frac{u_i^j}{k_i^j}\right)^{n_i^j}}, \tag{S44}$$

We assume that the free amount of both RNAPs and ribosomes are very limited, in particular:

$$y \ll K_i^j, K_i^0, K_i^{12} \ \ (j = 1, 2) \qquad \text{and} \qquad z \ll \kappa_i, \tag{S45}$$

In this situation, the concentration of active open complex for node i transcription becomes:

$$C_i = p_{i,T} \frac{\frac{y}{K_i^0} + \frac{y\hat{k}_i}{K_i^{12}} \left(\frac{u_i^1}{k_i^1}\right)^{n_i^1} \left(\frac{u_i^2}{k_i^2}\right)^{n_i^2} + \sum_{j=1,2} \frac{y}{K_i^j} \left(\frac{u_i^j}{k_i^j}\right)^{n_i^j}}{1 + \hat{k}_i \left(\frac{u_i^1}{k_i^1}\right)^{n_i^1} \left(\frac{u_i^2}{k_i^2}\right)^{n_i^2} + \sum_{j=1,2} \left(\frac{u_i^j}{k_i^j}\right)^{n_i^j}}. \tag{S46}$$

Setting ODEs (S39e) and (S39f) to QSS we obtain

$$M_i = \frac{\alpha_i}{\delta_i} \frac{z}{\kappa_i} C_i = \frac{p_{i,T} \alpha_i y z}{\delta_i \kappa_i} \cdot \frac{\frac{1}{K_i^0} + \frac{\hat{k}_i}{K_i^{12}} \left(\frac{u_i^1}{k_i^1}\right)^{n_i^1} \left(\frac{u_i^2}{k_i^2}\right)^{n_i^2} + \sum_{j=1,2} \frac{1}{K_i^j} \left(\frac{u_i^j}{k_i^j}\right)^{n_i^j}}{1 + \hat{k}_i \left(\frac{u_i^1}{k_i^1}\right)^{n_i^1} \left(\frac{u_i^2}{k_i^2}\right)^{n_i^2} + \sum_{j=1,2} \left(\frac{u_i^j}{k_i^j}\right)^{n_i^j}}, \tag{S47}$$

where $\kappa_i$ is the effective dissociation constant of RBS of node i binding with ribosomes:

$$\kappa_i = \frac{\kappa_i^- + \theta_i + \omega_i}{\kappa_i^+}.$$

In order to obtain physically relevant parameters and simplify our notation, we rearrange the expressions in (S47). Consider a Hill-type-function of the form

$$f(v, w) = \frac{\pi_0 + \pi_1 v^n + \pi_2 w^m + \pi_3 \lambda v^n w^m}{1 + v^n + w^m + \lambda v^n w^m}, \tag{S48}$$

where $\pi_0, \cdots, \pi_3$, $\lambda$, $n$ and $m$ are non-negative constants, and $v, w \in [0, \infty)$. Defining $\bar{\pi} := \max\{\pi_0, \pi_1, \pi_2, \pi_3\}$, notice that we have $\sup[f(v, w)] = \bar{\pi}$. Applying this result to the (S47), we define,

$$\bar{K}_i = \min\{K_i^0, K_i^1, K_i^2, K_i^{12}\},$$

so that we can re-write equation (S47) as

$$M_i = \frac{p_{i,T} \alpha_i y z}{\delta_i \kappa_i \bar{K}_i} \cdot F_i(\mathbf{u}_i) \tag{S49}$$

The function $F_i(\mathbf{u}_i) : \mathbb{R}_+^2 \mapsto [0, 1]$ describes the effect of TFs $u_i^1$ and $u_i^2$ on transcription of node i, it can be written as:

$$F_i(\mathbf{u}_i) = \frac{\beta_i^0 + \beta_i^{12} \hat{k}_i \left(\frac{u_i^1}{k_i^1}\right)^{n_i^1} \left(\frac{u_i^2}{k_i^2}\right)^{n_i^2} + \sum_{j=1,2} \beta_i^j \left(\frac{u_i^j}{k_i^j}\right)^{n_i^j}}{1 + \hat{k}_i \left(\frac{u_i^1}{k_i^1}\right)^{n_i^1} \left(\frac{u_i^2}{k_i^2}\right)^{n_i^2} + \sum_{j=1,2} \left(\frac{u_i^j}{k_i^j}\right)^{n_i^j}}, \tag{S50}$$

where

$$\beta_i^0 := \frac{\bar{K}_i}{K_i^0}, \qquad \beta_i^j := \frac{\bar{K}_i}{K_i^j}, \qquad \beta_i^{12} := \frac{\bar{K}_i}{K_i^{12}}.$$

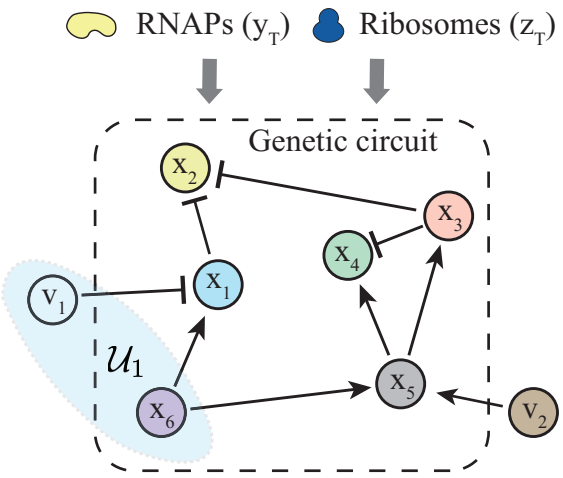


Figure S8: An example genetic circuit, with 6 nodes and 2 external TF inputs. A limited amount of RNAPs and ribosomes are available for nodes 1 to 6. Links between nodes indicate transcriptional regulation interactions, where "$\rightarrow$" is an activation and "$\dashv$" is a repression.

Equation (S50) is independent of the availability of resources and encapsulates the most common forms of transcriptional regulations. For example, when node i takes a single activator $\mathrm{u}_i^1$ as input, we have $\beta_i^0 < 1$, $\beta_i^1 = 1$, and $\beta_i^2 = \beta_i^{12} = 0$; when node i takes a single repressor $\mathrm{u}_i^1$ as input, we have $\beta_i^0 = 1$, $\beta_i^1 < 1$, and $\beta_i^2 = \beta_i^{12} = 0$; when node i is constitutive, $\beta_i^0 = 1$, and $\beta_i^1 = \beta_i^2 = \beta_i^{12} = 0$; when node i takes two competitive repressors $\mathrm{u}_i^1$ and $\mathrm{u}_i^2$ as input, $\beta_i^0 = 1$, $\beta_i^1, \beta_i^2 < 1$ and $\beta_i^{12} = 0$. Finally, we combine equations (S49) and (S39g) to obtain the dynamics of $x_i$:

$$\dot{x}_i = \frac{\alpha_i \theta_i p_{i,T}}{\delta_i} \cdot \frac{y}{\bar{K}_i} \cdot \frac{z}{\kappa_i} \cdot F_i(\mathbf{u_i}) - \gamma_i \cdot x_i. \tag{S51}$$

Since y and z are shared among all nodes in the network, their free concentrations $y$, $z$ need to be determined from the network context. This is discussed in the next subsection.

## B4.2 Resource sharing in genetic circuits

A genetic circuit is composed of $N$ nodes and $L$ external TF inputs $(\mathrm{v}_1, \cdots, \mathrm{v}_\mathrm{L})$. The concentrations of the external inputs can be represented by $\mathbf{v} = [v_1, \cdots, v_L]^T$ and the state of the network is represented by the concentrations of output proteins of each node $\mathbf{x} = [x_1, \cdots, x_N]^T$. The set of all TFs in the network is $\mathcal{X} = \{\mathrm{x}_1, \cdots, \mathrm{x}_\mathrm{N}, \mathrm{v}_1, \cdots, \mathrm{v}_\mathrm{L}\}$, and we use $\boldsymbol{\xi} = [\mathbf{x}^T, \mathbf{v}^T]^T \in \mathbb{R}^{(N+L)}$ to represent the vector of their concentrations. Nodes can be connected by regulatory interactions where protein $\mathrm{x_j}$ can either activate or repress the production of $\mathrm{x_i}$ by binding to its promoter. We call $\mathrm{x_i}$ as a *target* of $\mathrm{x_j}$ and $\mathrm{x_j}$ as a *parent* of $\mathrm{x_i}$. We denote by $\mathcal{U}_i \subseteq \mathcal{X}$ the set of all parents of $\mathrm{x_i}$. Their concentrations are given by a vector $\mathbf{u}_i = Q_i \cdot \boldsymbol{\xi}$, where $Q_i \in \mathbb{R}^{2\times(N+L)}$ is a selection matrix whose elements are defined as:

$$q_{jk} = \begin{cases} 1, & \text{if } \xi_k \text{ is the } j\text{th input to node i,} \\ 0, & \text{otherwise.} \end{cases}$$

Figure S8 illustrates an example genetic circuit. In this example circuit, $\mathbf{x} = [x_1, \cdots, x_6]^T$ and $\mathbf{v} = [v_1, v_2]^T$. Therefore, $\mathcal{X} = \{\mathrm{x}_1, \cdots \mathrm{x}_6, \mathrm{v}_1, \mathrm{v}_2\}$, and $\boldsymbol{\xi} = [x_1, \cdots, x_6, v_1, v_2]^T$. Using node 1 as an example, we have $\mathcal{U}_1 = \{\mathrm{x}_6, \mathrm{v}_1\}$, $\mathbf{u_1} = [x_6, v_1]^T$, and the selection matrix $Q_i \in \mathbb{R}^{2\times 8}$ can be written as

$$Q_i = \begin{bmatrix} 0 & 0 & 0 & 0 & 0 & 1 & 0 & 0 \\ 0 & 0 & 0 & 0 & 0 & 0 & 1 & 0 \end{bmatrix}.$$

As an extension of resource conservation in an activation cascade (S15), here, we have:

$$y_T = y + \sum_{i=1}^{N} y_i, \qquad\qquad z_T = z + \sum_{i=1}^{N} z_i. \tag{S52}$$

We let $y_i$ and $z_i$ denote the amount of RNAPs and ribosomes bound to node i:

$$y_i = C_i^0 + C_i^1 + C_i^2 + C_i^{12}, \qquad\qquad z_i = M_i.$$

According to (S46) and (S47), we use (S50) to simplify the notation for the resources bound to node i:

$$y_i = C_i = \frac{p_{i,T} y}{\bar{K}_i} F_i(\mathbf{u}_i), \qquad\qquad z_i = M_i = \frac{p_{i,T}\alpha_i y z}{\delta_i \kappa_i \bar{K}_i} F_i(\mathbf{u}_i) \tag{S53}$$

Combining equations (S52) and (S53), we obtain:

$$y = \frac{y_T}{1 + \sum_{i=1}^{N} [\frac{p_{i,T}}{\bar{K}_i} F_i(\mathbf{u}_i)]}, \qquad\qquad z = \frac{z_T}{1 + y \sum_{i=1}^{N} [\frac{\alpha_i p_{i,T}}{\delta_i \bar{K}_i \kappa_i} F_i(\mathbf{u}_i)]}.$$

Hence,

$$y \cdot z = \frac{y_T \cdot z_T}{1 + \sum_{i=1}^{N} \frac{p_{i,T}}{\bar{K}_i} \cdot (1 + \frac{\alpha_i}{\kappa_i \delta_i} y_T) \cdot F_i(\mathbf{u}_i)}. \tag{S54}$$

Substituting (S54) into (S51), we derive the dynamics of node i as:

$$\dot{x}_i = \frac{T_i F_i(\mathbf{u}_i)}{1 + \sum_{k=1}^{N} J_k F_k(\mathbf{u}_k)} - \gamma_i x_i, \tag{S55}$$

where $J_i$ and $T_i$ are lumped parameters defined as:

$$J_i := \frac{p_{i,T}}{\bar{K}_i} \cdot (1 + \frac{\alpha_i}{\kappa_i \delta_i} y_T), \qquad\qquad T_i := y_T z_T p_{i,T} \cdot \frac{\theta_i \alpha_i}{\bar{K}_i \kappa_i \delta_i}. \tag{S56}$$

$F_i(\mathbf{u}_i)$ is the only element in equation (S55) that reflects regulatory interactions on node i. According to equation (S50), the form of $F_i(\mathbf{u}_i)$ is the same as that of the standard Hill functions described in [12] and [13]. Notice that regardless of the nature of regulatory interaction (*i.e.* activation vs. repression), we always have $\sup[F_i(\mathbf{u}_i)] = 1$, hence, according to (S56), $T_i$ represents the maximal gene expression rate of node i, because $T_i$ is the production rate of $\mathrm{x_i}$ when $F_i(\mathbf{u}_i) = 1$, $y = y_T$ and $z = z_T$.

To demonstrate the effectiveness of our general model, we apply it to a simple genetic circuit used previously to study resource competition between an inducible gene and a constitutive one in [16, 1]. The effective interaction graph of this circuit is reproduced in Figure S9. In this circuit, a TF u is transcriptionally activating the production of protein $\mathrm{x_1}$. Another protein $\mathrm{x_2}$ is produced constitutively. Experimental results in [16, 1] indicate that at steady state, due to competition for a limited pool of RNAPs and ribosomes, the steady state concentrations of $\mathrm{x_1}$ and $\mathrm{x_2}$ follow a linear relationship:

$$a\bar{x}_1 + b\bar{x}_2 = 1.$$

This result can be shown as a special case of our general model (S55). According to (S55), gene expressions in this circuit can be written as:

$$\dot{x}_1 = \frac{T_1 F_1(u)}{1 + J_1 F_1(u) + J_2} - \gamma_1 x_1, \qquad\qquad \dot{x}_2 = \frac{T_2}{1 + J_1 F_1(u) + J_2} - \gamma_2 x_2.$$

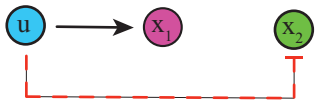


Figure S9: A genetic circuit consists of an inducible gene and a constitutive gene. Due to resource competition, steady state expression levels $\bar{x}_1$ and $\bar{x}_2$ follow a linear relationship called "isocost line" [1].

At steady state, when expression of the two nodes are $\bar{x}_1$ and $\bar{x}_2$, respectively, we have

$$\bar{x}_1 = \frac{T_1 F_1(u)}{\gamma_1[1 + J_1 F_1(u) + J_2]}, \qquad \bar{x}_2 = \frac{T_2}{\gamma_2[1 + J_1 F_1(u) + J_2]}. \tag{S57}$$

From (S57), we find

$$\underbrace{\frac{J_1\gamma_1}{T_1}}_{a}\bar{x}_1 + \underbrace{\frac{(1+J_2)\gamma_2}{T_2}}_{b}\bar{x}_2 = 1,$$

where parameters $a$ and $b$ are equivalent to the ones in the previous model [1].

Indeed, the circuit in Figure S9 can be viewed as an extreme case of the activation cascade we studied in this paper, with the second activation stage $x_1 \to x_2$ negligibly weak. This situation happens, for example, when activation of $x_2$ by $x_1$ is saturated, while expression of $x_1$ continues to deplete resources as $u$ increases, effectively inhibiting $x_2$ expression. The monotonically decreasing or biphasic response curve of the activation cascade thus becomes not surprising.

## B5 $J_i$ quantifies resource demand in node i

$J_i$ is a dimensionless lump parameter for node i that defines its maximal resource demand when $F_i(\mathbf{u}_i) = 1$. We take $J_i$ as a measure of resource demand by node i because the expression in equation (S54) implies the "conservation law" for $y \cdot z$:

$$y_T \cdot z_T = \underbrace{y \cdot z}_{\text{free resources}} + \sum_{i=1}^{N} \underbrace{[J_i \cdot F_i(\mathbf{u}_i)] \cdot y \cdot z}_{\text{resources bound to node } i}. \tag{S58}$$

Furthermore, the major between our model in equation (S22) and the standard Hill function model in (S10) is the common denominator term $\mathcal{D} = 1 + \sum_{k=1}^{N} J_k F_k(\mathbf{u}_k)$. The following claim shows that when resources bound to the nodes are negligibly small, the resource demand measures for all nodes must satisfy $J_i \ll 1$ for all $i$.

**Claim 3.** *For every $\mathbf{u}_i$, if $y_i \ll y$ and $z_i \ll z$ for all $i = 1, \cdots, N$, then $J_i \ll 1$ for all $i = 1, \cdots, N$.*

*Proof.* Using equation (S53), $y_i \ll y$ for every $\mathbf{u}_i$ is requires $p_{i,T} F_i(\mathbf{u}_i)/\bar{K}_i < p_{i,T}/\bar{K}_i \ll 1$, since $F_i(\mathbf{u}_i) \leq 1$. Similarly, $z_i \ll z$ for every $\mathbf{u}_i$ requires $\frac{\alpha_i p_{i,T} y}{\delta_i \bar{K}_i \kappa_i} \ll 1$. Since $y_i \ll y$ for all $i$, $y \approx y_T$. Therefore, $\frac{\alpha_i p_{i,T} y_T}{\delta_i \bar{K}_i \kappa_i} \ll 1$ and $J_i \ll 1$ for all $i$. □

This claim shows that when resource demand is negligible in the network, $0 < J_i \ll 1$ ($i = 1, \cdots, N$), our model (S22) reduces to the standard Hill-function model in (S10). Equation (S56) indicates that a node i is a strong resource sequester if its (i) copy number is large; (ii) RNAP sequestering capability is strong (small $\bar{K}_i$); (iii) transcription rate constant is large; (iv) ribosome

sequestering capability is strong (small $\kappa_i$); (v) mRNA degradation rate is low or (vi) the total amount of RNAP is large. Conditions (i) and (ii) are associated with the $p_{i,T}/\bar{K}_i$ term in equation (S56), and describe the node's capability to occupy RNAP. Conditions (iii) to (vi) are considered from the $(\alpha_i y_T)/(\kappa_i \delta_i)$ term and characterize the node's capability to occupy ribosomes.

## B6 Rules to draw effective interaction graphs

Directed edges, such as those in Figure S8, have been used to represent regulatory interactions among nodes in genetic circuits [12]. In this section, we expand their applications to represent interactions in a circuit with both regulatory interactions and non-regulatory interactions arising from resource competitions. These rules allow us to easily obtain the effective interactions among nodes, presented in Figure 4 of the main text. We first mathematically define the standards to draw directed edges in a genetic circuit, and then obtain effective interactions among nodes based on our model in equation (S55).

**Definition 1.** Let the dynamics of $x_i$ be given by $\dot{x}_i = G_i(\boldsymbol{\xi}) - \gamma_i \cdot x_i$. We draw the interaction graph from TF $\xi_{\mathrm{j}}$ to $\mathrm{x_i}$ based on the following rules:

- If $\frac{\partial G_i}{\partial \xi_j} \equiv 0$ for all $\xi_j \in \mathbb{R}_+$, then there is no interaction from $\xi_{\mathrm{j}}$ to $\mathrm{x_i}$;
- If $\frac{\partial G_i}{\partial \xi_j} \geq 0$ for all $\xi_j \in \mathbb{R}_+$ and $\frac{\partial G_i}{\partial \xi_j} \neq 0$ for some $\xi_j$, then $\xi_{\mathrm{j}}$ activates $\mathrm{x_i}$ and we draw $\xi_{\mathrm{j}} \to \mathrm{x_i}$;
- If $\frac{\partial G_i}{\partial \xi_j} \leq 0$ for all $\xi_j \in \mathbb{R}_+$ and $\frac{\partial G_i}{\partial \xi_j} \neq 0$ for some $\xi_j$, then $\xi_{\mathrm{j}}$ represses $\mathrm{x_i}$ and we draw $\xi_{\mathrm{j}} \dashv \mathrm{x_i}$.
- If $\frac{\partial G_i}{\partial \xi_j} \geqslant 0$ for some $\xi_j \in \mathbb{R}_+$ and $\frac{\partial G_i}{\partial \xi_j} < 0$ for some other $\xi_j$, then the regulation of $\xi_{\mathrm{j}}$ on $\mathrm{x_i}$ is undetermined and we draw $\xi_{\mathrm{j}} \multimap \mathrm{x_i}$;

Based on Definition 1, for the standard model in equation (S10), $G_i(\boldsymbol{\xi}) = T_i F_i(Q_i \boldsymbol{\xi}) = T_i F_i(\mathbf{u}_i)$, and therefore there is a link from $\xi_{\mathrm{j}}$ to $\mathrm{x_i}$ if and only if $\xi_{\mathrm{j}} \in \mathcal{U}_i$. In our model (S22), instead we have

$$G_i(\boldsymbol{\xi}) = \frac{T_i F_i(Q_i \cdot \boldsymbol{\xi})}{1 + \sum_{k=1}^{N} J_k F_k(Q_k \cdot \boldsymbol{\xi})} = \frac{T_i F_i(\mathbf{u}_i)}{1 + \sum_{k=1}^{N} J_k F_k(\mathbf{u}_k)},$$

which implies that the dynamics of $x_i$ may be influenced by TFs that do not belong to $\mathcal{U}_i$.

In what follows, we discuss the effective interactions from $\xi_{\mathrm{j}} \in \chi$ to protein $\mathrm{x_i}$ when (i) $\mathrm{x_i}$ is the only target of $\xi_{\mathrm{j}}$, (ii) $\mathrm{x_i}$ is one of the multiple targets of $\xi_{\mathrm{j}}$, and (iii) $\mathrm{x_i}$ is not a target of $\xi_{\mathrm{j}}$. We do not require $\mathrm{x_i} \neq \xi_{\mathrm{j}}$ and assume that a TF cannot be both an activator and a repressor. When $\mathrm{x_i}$ is the only target of $\xi_{\mathrm{j}}$, the following claim shows that resource limitations do not alter the activation/repression of $\mathrm{x_i}$ by $\xi_{\mathrm{j}}$ in the interaction graph.

**Claim 4.** If $\xi_{\mathrm{j}} \in \mathcal{U}_i$ and $\xi_{\mathrm{j}} \notin \mathcal{U}_q$ for all $(q \neq i)$. Then we have $\mathrm{sign}[\partial G_i(\boldsymbol{\xi})/\partial \xi_j] = \mathrm{sign}[\partial F_i(Q_i \boldsymbol{\xi}))/\partial \xi_j]$.

*Proof.* According to equation (S22),

$$\frac{\partial G_i(\boldsymbol{\xi})}{\partial \xi_j} = \overbrace{\frac{\partial G_i}{\partial F_i}}^{\text{positive}} \cdot \frac{\partial F_i(Q_i \boldsymbol{\xi})}{\partial \xi_j} \Rightarrow \mathrm{sign}\left(\frac{\partial G_i}{\partial \xi_j}\right) = \mathrm{sign}\left(\frac{\partial F_i}{\partial \xi_j}\right).$$

□

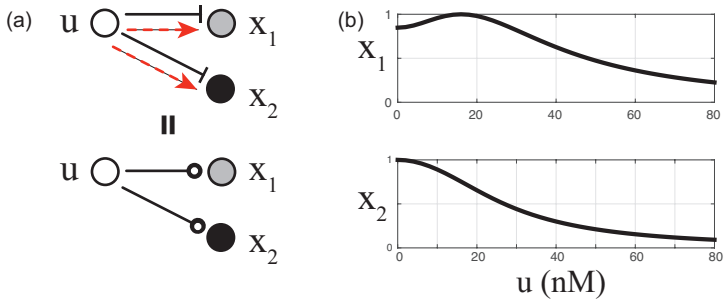


Figure S10: **Lateral activation by a repressor.** (a) Effective interaction graph of a single-input motif [12]. Black arrows represent regulatory interactions and red dashed arrows represent non-regulatory interactions due to resource competition. (b) Dose response curves of the circuit in (a). Expression level of $x_1$ is nomonotonic with respect to u, which is its repressor.

In the case where $\xi_j \in \mathcal{U}_1, \cdots, \mathcal{U}_k$ $(k \geq 2)$, the effective interactions from $\xi_j$ to its targets are undetermined. For example, if $\xi_j$ represses $x_1$ and $x_2$ simultaneously, the effective interaction from $\xi_j$ to $x_1$ is given by

$$\frac{\partial G_1(\boldsymbol{\xi})}{\partial \xi_j} = \underbrace{\frac{\partial G_1}{\partial F_1}}_{\text{positive}} \cdot \overbrace{\underbrace{\frac{\partial F_1(Q_1\boldsymbol{\xi})}{\partial \xi_j}}_{\text{negative}}}^{\text{transcriptional repression}} + \overbrace{\underbrace{\frac{\partial G_1}{\partial F_2}}_{\text{negative}} \cdot \underbrace{\frac{\partial F_2(Q_2\boldsymbol{\xi})}{\partial \xi_j}}_{\text{negative}}}^{\text{hidden activation}}. \tag{S59}$$

As $\text{sign}(\partial G_1/\partial \xi_j)$ cannot be determined, the effective interaction from $\xi_j$ to $x_1$ is undetermined. Simulation of this situation is presented in Figure S10. In Figure S10(a), we present the effective interaction graph of a single-input motif, where TF u transcriptionally represses two targets $x_1$ and $x_2$. The nature of effective interactions from u to $x_1$ and $x_2$ are undetermined. In particular, in Figure S10, we simulated a situation where dose response of $x_1$ with respect to u becomes biphasic, rather than the intended monotonically decreasing. This situation is captured by equation (S59). Physically, this fact can be explained by the following resource competition mechanism: if $x_2$ occupies a lot of resources in the absence of u (large $J_2$), a large amount of resources are released in the presence of u, effectively promoting the expression of $x_1$.

When $\xi_j$ is not a parent of $x_i$, the following claim shows $\xi_j$ is an effective repressor for $x_i$ if $\xi_j$ is an activator. Conversely, $\xi_j$ is an effective activator for $x_i$ if it is a repressor.

**Claim 5.** If $\xi_j \notin \mathcal{U}_i$ but $\xi_j \in \mathcal{U}_k$ for some $k \neq i$, then we have $\text{sign}[\partial G_i(\boldsymbol{\xi})/\partial \xi_j] = -\text{sign}[\partial F_k(Q_k\boldsymbol{\xi})/\partial \xi_j]$.

*Proof.* Since $\xi_j \notin \mathcal{U}_i$, $\partial G_i/\partial F_k < 0$ for all $k$.

$$\frac{\partial G_i(\boldsymbol{\xi})}{\partial \xi_j} = \sum_k \underbrace{\frac{\partial G_i}{\partial F_k}}_{\text{negative}} \cdot \frac{\partial F_k(Q_k\boldsymbol{\xi})}{\partial \xi_j}.$$

Therefore, $\text{sign}(\partial G_i/\partial \xi_j) = -\text{sign}(\partial F_k/\partial \xi_j)$. □

All results in this section are summarized in Figure 4 of the main text.

## B7 Dose response of a two-stage repression cascade

Here, we consider an application of our general model and graphical rules obtained in Sections B4 and B6 to another circuit commonly used for biological signal transduction and amplification: a two-stage repression cascade. A two-stage repression cascade consists of a TF input u transcriptionally repressing $x_1$, which is a repressor of the output protein $x_2$. As $u$ increases, concentration of $x_2$

increases due to reduced amount of $x_1$. When this circuit is subject to resource competition, its ODE model can be written, according to (S55), as

$$\begin{aligned}\dot{x}_1 &= \frac{T_1 F_1(u)}{1 + J_1 F_1(u) + J_2 F_2(x_1)} - \gamma_1 x_1,\\ \dot{x}_2 &= \frac{T_2 F_2(x_1)}{1 + J_1 F_1(u) + J_2 F_2(x_1)} - \gamma_2 x_2,\end{aligned} \tag{S60}$$

where

$$F_1(u) = \frac{1}{1 + \left(\frac{u}{k_1}\right)^{n_1}} \qquad F_2(x_1) = \frac{1}{1 + \left(\frac{x_1}{k_2}\right)^{n_2}}. \tag{S61}$$

According to Claim 1, slope of its dose response curve $\mathrm{d}\bar{x}_2/\mathrm{d}u$ can be found as

$$\frac{\mathrm{d}\bar{x}_2}{\mathrm{d}u} = H(0) = \frac{\frac{\partial G_2}{\partial x_1} \cdot \frac{\partial G_1}{\partial u} + \left(\gamma_1 - \frac{\partial G_1}{\partial x_1}\right) \cdot \frac{\partial G_2}{\partial u}}{\left(\gamma_1 - \frac{\partial G_1}{\partial x_1}\right) \gamma_2}, \tag{S62}$$

with

$$G_1(u, x_1) = \frac{T_1 F_1(u)}{1 + J_1 F_1(u) + J_2 F_2(x_1)}, \qquad G_2(u, x_1) = \frac{T_2 F_2(x_1)}{1 + J_1 F_1(u) + J_2 F_2(x_1)}.$$

Note that the expression of the slope in (S62) for the repression cascade is identical to that of the activation cascade in (S30). However, here, since the Hill functions ($F_1(u)$ and $F_2(x_1)$) now decrease with their arguments, we have

$$\frac{\partial G_1}{\partial u} = \underbrace{\frac{\partial G_1}{\partial F_1}}_{\text{positive}} \cdot \underbrace{\frac{\partial F_1}{\partial u}}_{\text{negative}} < 0, \qquad \frac{\partial G_1}{\partial x_1} = \underbrace{\frac{\partial G_1}{\partial F_2}}_{\text{negative}} \cdot \underbrace{\frac{\partial F_2}{\partial x_1}}_{\text{negative}} > 0,$$

$$\frac{\partial G_2}{\partial u} = \underbrace{\frac{\partial G_2}{\partial F_1}}_{\text{negative}} \cdot \underbrace{\frac{\partial F_1}{\partial u}}_{\text{negative}} > 0, \qquad \frac{\partial G_2}{\partial x_1} = \underbrace{\frac{\partial G_2}{\partial F_2}}_{\text{positive}} \cdot \underbrace{\frac{\partial F_2}{\partial x_1}}_{\text{negative}} < 0.$$

Consequently, as long as $\gamma_1 > |\partial G_1/\partial x_1|$, we have $H(0) > 0$, and the slope of the dose response curve of a repression is always positive. This property of the repression cascade can also be explained by the effective interaction graph we presented in Figure 4D of the main text. Since u is a repressor, with $x_1$ being its only target, the effective interaction between u and $x_1$ is still repression, and the effective interaction between u and $x_2$ is an activation. Similarly, according to the rules established in Figure 4A-C, the effective interaction from $x_1$ to $x_2$ is a repression, while $x_1$ is also effectively activating itself. The two interactions acting from u to $x_2$ are both effective activations: $u \dashv x_1 \dashv x_2$ and $u \to x_2$. Therefore, steady state of $x_2$ is guaranteed to increase with $u$. Situations where $\gamma_1 > |\partial G_1/\partial x_1|$ corresponds to scenarios where the repression cascade becomes bistable due to the hidden self-activation loop $x_1 \to x_1$. Self-activation loops are closely related to bistability in genetic circuits [12, 13]. While existing experimental results have illustrated repression cascades to show bimodal behavior [17], whether the observed bimodality is due to bistability arising from the non-regulatory self-activation still needs to be investigated.

## B8 Effects of additional constitutive nodes on effective interactions

In the main text of this paper, we study a model of the two-stage activation cascade that does not take into account resource demand by the constitutive gene *luxR*, and only considers competition for resources between NahR and GFP. Here, we extend our model to explicitly account for resource

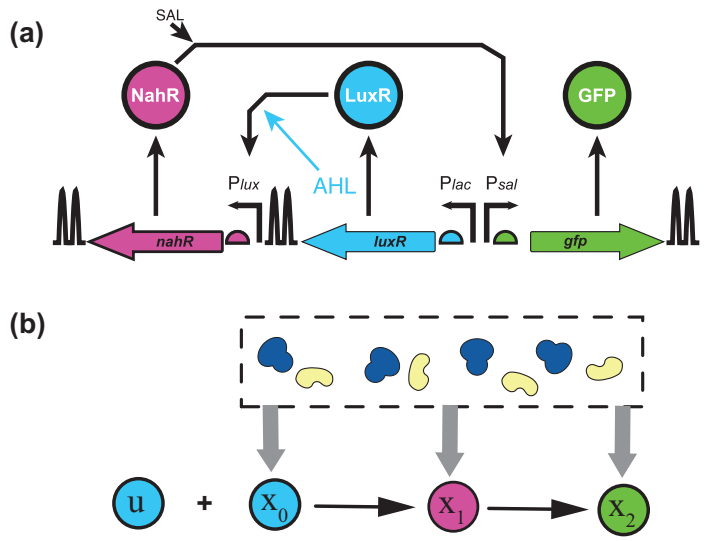


Figure S11: (a) Two-stage activation, reproduced from Figure 1 of the main text. (b) Schematic of the activation cascade with a constitutive node $x_0$. A conserved amount of resources are used to produce the constitutive node $x_0$, and the two stages of the activation cascade $x_1$ and $x_2$.

demand of *luxR*, which we call node 0. We show that whether this constitutive node is included in the resource competition model or not does not change our qualitative results on the shape of dose response curves. A schematic of the circuit with the constitutive node $x_0$ is shown in Figure S11.

According to (S55), an ODE model of the system is:

$$\begin{aligned}\dot{x}_1 &= \frac{T_1 F_1(u)}{1 + J_0 F_0 + J_1 F_1(u) + J_2 F_2(x_1)} - \gamma_1 x_1,\\ \dot{x}_2 &= \frac{T_2 F_2(x_1)}{1 + J_0 F_0 + J_1 F_1(u) + J_2 F_2(x_1)} - \gamma_2 x_2.\end{aligned}$$

Since node 0 is constitutive, we have $F_0 \equiv 1$. Consequently, the model can be written as

$$\begin{aligned}\dot{x}_1 &= \frac{\tilde{T}_1 F_1(u)}{1 + \tilde{J}_1 F_1(u) + \tilde{J}_2 F_2(x_1)} - \gamma_1 x_1,\\ \dot{x}_2 &= \frac{\tilde{T}_2 F_2(x_1)}{1 + \tilde{J}_1 F_1(u) + \tilde{J}_2 F_2(x_1)} - \gamma_2 x_2,\end{aligned} \tag{S63}$$

where we have defined the following new lumped parameters:

$$\tilde{T}_i = \frac{T_i}{1 + J_0}, \qquad \tilde{J}_i = \frac{J_i}{1 + J_0}, \qquad (i = 1, 2). \tag{S64}$$

Note that equation (S63) has the same form as (S22), which is the model we derived only considering resource competition between node 1 and 2. Therefore, we may conclude that adding a constitutive $x_0$ to the circuit is equivalent to changing parameters $T_i$ and $J_i$ $(i = 1, 2)$. The properties of non-regulatory interactions arising resource competition is unaffected, and we would expect that the dose response curves can be positive, negative or biphasic. Note that according to (S64), the resource demand $J_1$ and $J_2$ of both nodes decrease with $J_0$. Since small $J_1$ guarantees monotonically increasing dose response curve of the activation cascade, a constitutive node 0 with large resource demand can be used as a sponge to passively mitigates the effects of resource competition on circuit behavior. The price, however, is that expression of all genes in the circuit will be quenched due to decreased $T_1$ and $T_2$. Interestingly, such strategy maybe used by natural systems to deal with fluctuation in RNAP concentrations [18].

## B9 Parametric analysis

We follow the widely used convention that a concentration of 1 molecule/cell is equivalent to a concentration of 1 nM, due to the fact that typical volume of an *E. coli* cell is $10^{-18}$ $m^3$ [19]. Therefore, the total concentration of the promoters are given by plasmid copy number as $p_{1,T} = p_{2,T} = 30$ nM for CAS 1/30 and CAS 0.3/30, and $p_{1,T} = p_{2,T} = 60$ nM for CAS 1/60 and CAS 0.3/60. According to [5], elongation rate constant of mRNA chain is about 30 nucleotides per second, and GFP has about 720 nucleotides, transcribing each gene takes about half a minute. We therefore take transcription rate constant to be $\alpha_i \approx 100$ $hr^{-1}$. According to [20], each DNA can have as many as 20 RNAPs transcribing simultaneously. This fact is critical to our model as the number of RNAPs engaged in the transcription of gene i can be significantly larger than assuming a single RNAP binding to the promoter. To account for this fact in our model, instead of assuming each gene can bind with $\lambda$ RNAPs, we assume that the plasmid copy numbers are increased by a factor of $\lambda$, while each promoter can only bind a single RNAP. In this way, the binding kinetics between promoters and RNAPs are unaffected, but effective RNAP demand and mRNA production increased. Here, we take a conservative estimate that $\lambda = 5$, so effective total promoter concentration of gene i is $\lambda p_{i,T}$. Similarly, elongation rate of the peptide chain is about 10 amino acid per second, and a typical GFP has 250 amino acid, translating its mRNA takes about half a minute. We therefore estminate $\theta_i \approx \alpha_i \approx 100$ $hr^{-1}$. Each mRNA can have as many as 30 ribosomes translating simultaneously [21]. These multi-ribosome complexes are also known as "polysomes", which can significantly increase ribosome demand of a circuit. Instead of modeling each mRNA binding $\phi$ ribosomes, we model it as the number of mRNAs increased by a factor of $\phi$, and each of them only binds one ribosome. Increase in the number of mRNAs can be modeled by increasing the transcription rate constant $\alpha_i$ by $\phi$ times. The half life time of mRNA ranges ranges from 3 to 10 minutes, we estimate its decay rate $\delta_i$ to be between $4 \sim 15$ $texthr^{-1}$. When ribosomes are bound to mRNAs, they protect the mRNAs from degradation [22], we therefore assume $\omega_i < \delta_i$. The decay rate of proteins are set to be $\gamma_i \approx 0.4$ $hr^{-1}$ to be consistent with experimental observations.

The dissociation constants between TFs and target DNAs, $k_i$, can range between 0.02 nM to 10 µM, and that of RNAP binding non-specifically with DNA ($K_i^0$) is typically larger than 10 µM [23]. The dissociation constant of T7 RNAP binding with promoter is 220 nM [24]. T7 RNAP has stronger binding with promoters than other RNAP species [25], therefore, we expect $K >$220 nM. For instance, the dissociation constant of *lac* promoter with RNAP is about 550 nM [26]. A typical dissociation constant of ribosome binding with RBS is 5 µM [21]. Furthermore, notice that according to (S42), our definition of effective dissociation constants $K_i^0$, $K_i$ and $\kappa_i$ in node i is always larger than the standard definition of dissociation constant ($d_i/a_i$) due to the presence of transcription/translation elongation rate constant in the numerators.

The total amount of resource in *E. coli* cells is dependent on cell growth rate: slower growth rate indicates smaller total amount of resources [5]. In all our experiments with different activation cascades and AHL inputs, host cell growth were relatively slow. The maximum specific growth rate was obtained in CAS 0.3/30 experiment at about 0.5 per hour. Specific growth rates in other experiments were even slower at about $0.3 \sim 0.4$ per hour (see Figure S2). According to Bremer et.al. [5], at specific growth rate of about 0.4 per hour, the total number of RNAPs per *E. coli* cell is about 1500 molecules. The total amount of active ribosomes per *E. coli* cell is about 6000 molecules, of which about 5000 molecules are active. However, a large portion of RNAP and ribosomes are allocated to transcribe/translate endogenous circuits of the host cell. According to [27], in *E. coli* cells at specific growth rate of 0.7 per hour, the free amount of RNAP is about 150 molecules, and the amount of free ribosomes is about 1000 molecules. Since RNAPs and ribosomes are also sequestered by the synthetic activation cascade, and that we observed specific growth rates slower than 0.7 per hour, we expected the free amount of RNAPs and ribosomes in our experiments to be smaller than 150 nM and 1 µM, respectively. Therefore, based on the characteristic values of dissociation constant $K_i^0$, $K_i$ and $\kappa_i$, our limited resource assumptions in (S45) that $y \ll K_i, K_i^0$ and $z \ll \kappa_i$ are reasonable. As the size of synthetic circuit increases, the amount of free resources becomes more scare, and this assumption is closer to reality. Physically, these assumptions correspond to situations where the promoters are rarely occupied by RNAP and that mRNAs are in excess compared to free ribosomes, both of which are common in experiments [28, 29].

Table 1: Characteristic values of biological parameters

| Parameters | | Characteristic values | Sources |
|---|---|---|---|
| Total DNA concentration | $p_{i,T}$ | 1 copy $\sim$ 1 nM | [19] |
| Total RNAPs available to synthetic circuit | $y_T$ | $\lesssim$ 1000 nM | [1, 5, 27] |
| Total ribosomes available to synthetic circuit | $z_T$ | $\lesssim$ 1000 nM | [1, 5, 27] |
| Dissociation constant between TFs and DNAs | $k_i^j$ | $10^{-2} \sim 10^3$ nM | [23] |
| Dis. const. between RNAPs and DNAs (specific) | $K_i^j$ | $\gtrsim$ 500 nM | [24, 25, 26] |
| Dis. const. between RNAPs and DNAs (nonspecific) | $K_i^0$ | $\gtrsim$ 10 $\mu$M | [19] |
| Dis. const. between ribosomes and RBS | $\kappa_i$ | $\gtrsim$ 5 $\mu$M | [21] |
| Transcription elongation rate constant | $\alpha_i$ | $\sim$ 100 hr$^{-1}$ | [5] |
| Translation elongation rate constant | $\theta_i$ | $\sim$ 100 hr$^{-1}$ | [5] |
| Number of RNAPs per DNA | $\lambda$ | $\lesssim$ 20 | [20] |
| Number of ribosomes per mRNA | $\phi$ | $\lesssim$ 30 | [21] |
| mRNA decay rate constant | $\delta_i$ | $4 \sim 15$ hr$^{-1}$ | [19] |
| mRNA+ribosome complex decay rate constant | $\omega_i$ | $< \delta_i$ | [22] |
| Protein decay rate constant | $\gamma_i$ | $0.3 \sim 0.4$ hr$^{-1}$ | Experiment |

In fact, the total amounts of resources $y_T$ and $z_T$ available to the circuit of interest is not equal to the total amounts of resources reported in [5]. This is because a large portion of resources are allocated to express endogenous circuits of the host cell. If we regard the endogenous circuit as a constitutively expressed gene, with strong resource sequestration, then the total amounts of resources available to the synthetic circuit are approximately the free amounts. Moreover, with RNAPs and ribosomes unevenly distributed in cells in reality, recent experimental results have suggested that resource competition may be a local behavior [1, 30]. Based on the above reasoning, we argue that the total amount of resources available to the synthetic circuit is less than the free resources in the whole cell reported in [5, 27]. A summary of all characteristic parameters discussed in this section are summarized in Table 1.

## B10 Simulation implementations

To generate Figure 2, we simulate a full model of the activation cascade, which takes into account ODEs in (S1a)-(S1l) and the resource conservation law (S15). Simulations are performed by MATLAB R2014b (Simulink) with variable step ODE solver ode15s. Notice that we do not incorporate the limited resources assumption (S45) into our model. The assumption is only used to derive a lower dimensional model (S22) for the sake of mathematical analysis. However, simulation results still match predictions obtained by the lower dimensional analytical model (S22). Simulation parameters are listed in Table 2. Parameter values are chosen from typical parameter ranges reasoned in Section B9 to match the qualitative dose response curves observed in experiments.

Table 2: Simulation parameters to generate Figure 2

| Parameter | Unit | Value | Parameter | Unit | Value |
|---|---|---|---|---|---|
| $y_T$ | nM | 200 | $z_T$ | nM | 140 |
| $K_1^0$ | $\mu$M | 50 | $K_2^0$ | $\mu$M | 100 |
| $K_1$ | $\mu$M | 5 | $K_2$ | $\mu$M | 1 |
| $\delta_i$ | hr$^{-1}$ | 5 | $\omega_i$ | hr$^{-1}$ | 1 |
| $\theta_i$ | hr$^{-1}$ | 100 | $\alpha_i$ | hr$^{-1}$ | 100 |
| $n_1$ | - | 2 | $n_2$ | - | 4 |
| $k_1$ | nM | 10 | $k_2$ | nM | 200 |
| $\kappa_0$ | $\mu$M | 15 | $\kappa_2$ | $\mu$M | 15 |
| $\lambda = \phi$ | - | 5 | $\gamma_i$ | hr$^{-1}$ | 0.4 |

Sample dose response curves generated by activation cascades in the parameter space in Figure

2 is shown in Figure S12. The maximum amount of GFP output is about 7 µM when $p_{1,T} = p_{2,T}$=60 nM, and $\kappa_1 = \kappa_0/3$, a situation being comparable to CAS 1/60. The protein concentration is comparable to that of some common proteins in *E. coli* [19].

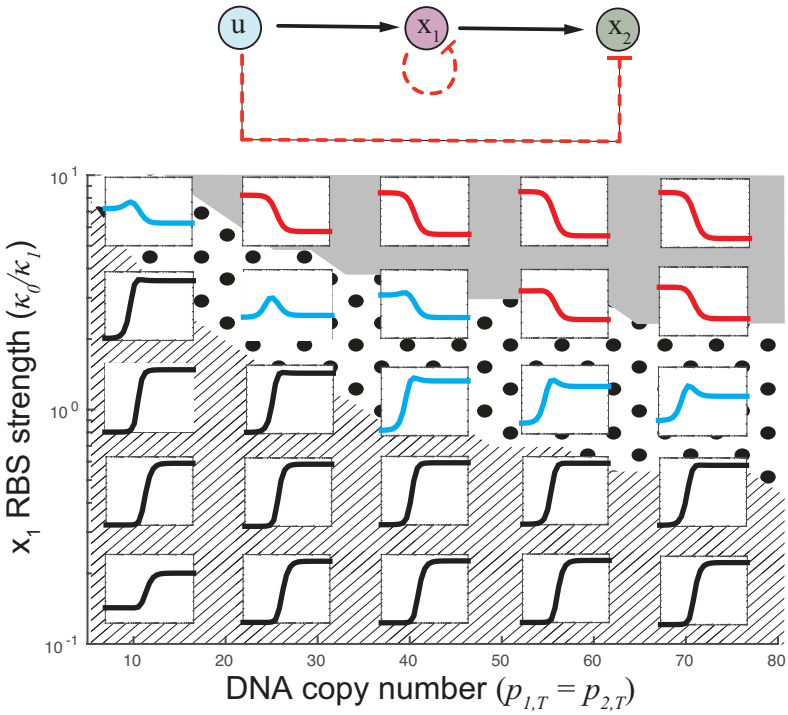


Figure S12: Sample dose response curves of activation cascades in the parameter space. Black dose response curves are monotonically increasing, cyan ones are biphasic and red ones are monotonically decreasing.

The purpose of this study is to qualitatively demonstrate the existence and significance of non-regulatory interactions due to resource competition, and to understand relevant biological parameters that govern their strengths. Since the existence and effects of non-regulatory interactions are independent of exact parameters, we did not attempt to fit the model to exact experimental results. Most likely, due to the large number of unknown parameters in the model, parameter fitting may result in multiple local optima. Furthermore, performing a satisfactory parameter fitting requires a few additional considerations, and therefore a more comprehensive model. These considerations include but are not limited to 1) binding reactions to form LuxR+AHL complex, 2) binding reactions to form NahR+SAL complex, 3) step-wise does response curve of transcription activation by NahR (see Section A5), whose detailed biomolecular mechanism is largely unclear, 4) dependence of the number of RNAPs/ribosomes simultaneously binding a DNA/mRNA molecule on RBS strength, DNA copy number and growth conditions, 5) change of dilution rate constants and total amount of resources due to slower growth rate in CAS 1/30 and CAS 1/60 experiments (see A4), and 6) the allocation of resources between a synthetic circuit and the endogenous circuits of the host cell, where many relevant biomolecular mechanisms remain unknown. In future work, we will study to what extent these additional considerations needs to be factored into the model.

# References

[1] Andras Gyorgy, José I. Jiménez, John Yazbek, Hsin-Ho Huang, Hattie Chung, Ron Weiss, and Domitilla Del Vecchio. Isocost lines describe the cellular economy of gene circuits. *Biophys. J.*, 109(3):639–646, 2015.

[2] D G Gibson, L Young, R Y Chuang, J C Venter, C A Hutchison 3rd, and H O Smith. Enzymatic assembly of DNA molecules up to several hundred kilobases. *Nature Methods*, 6(5):343–345, 2009.

[3] Joshua T Kittleson, Sherine Cheung, and J Christopher Anderson. Rapid optimization of gene dosage in E. coli using DIAL strains. *Journal of biological engineering*, 5(1):10, 2011.

[4] Olivier Borkowski, Francesca Ceroni, Guy-Bart Stan, and Tom Ellis. Overloaded and stressed: whole-cell considerations for bacterial synthetic biology. *Current Opinion in Microbiology*, 33:123 – 130, 2016.

[5] Hans Bremer and Patrick P. Dennis. Modulation of chemical composition and other parameters of the cell by growth rate. In Frederick C. Neidhardt, editor, *Escherichia coli and Salmonella: Cellular and Molecular Biology*. ASM Press, 1996.

[6] Francesca Ceroni, Rhys Algar, Guy-Bart Stan, and Tom Ellis. Quantifying cellular capacity identifies gene expression designs with reduced burden. *Nat. Methods*, 12(5):415–422, 2015.

[7] Thomas E Gorochowski, Irem Avcilar-kucukgoze, Roel A L Bovenberg, Johannes A Roubos, and Zoya Ignatova. A Minimal Model of Ribosome Allocation Dynamics Captures Trade- offs in Expression between Endogenous and Synthetic Genes. *ACS Synth. Biol.*, 5(7):710–720, 2016.

[8] Stefan Klumpp, Zhongge Zhang, and Terence Hwa. Growth-rate dependent global effect on gene expression in bacteria. *Cell*, 139:1366–1375, 2009.

[9] Stefan Klumpp. Mechanisms and economy of molecular machines. *Phys. Scr.*, T151:014066, 2012.

[10] Jianzhong Huang and Mark A. Schell. In vivo interactions of the NahR transcriptional activator with its target sequences: Inducer-mediated changes resulting in transcription activation. *Journal of Biological Chemistry*, 266(17):10830–10838, 1991.

[11] Hwi Park Hoo, Ki Lim Woon, and Hae J. Shin. In vitro binding of purified NahR regulatory protein with promoter Psal. *Biochimica et Biophysica Acta - General Subjects*, 1725(2):247–255, 2005.

[12] Uri Alon. *An Introduction to Systems Biology: Design Principles of Biological Circuits*. Chapman & Hall/CRC Press, 2006.

[13] Domitilla Del Vecchio and Richard M. Murray. *Biomolecular Feedback Systems*. Princeton University Press, Princeton, 2014.

[14] Jennifer A N Brophy and Christopher A Voigt. Principles of genetic circuit design. *Nat. Methods*, 11(5):508–520, 2014.

[15] Sara Hooshangi, Stephan Thiberge, and Ron Weiss. Ultrasensitivity and noise propagation in a synthetic transcriptional cascade. *Proc. Natl. Acad. Sci. U. S. A.*, 102(10):3584–3586, 2005.

[16] M. Carbonell-Ballestero, E. Garcia-Ramallo, R. Montañez, C. Rodriguez-Caso, and J. Macía. Dealing with the genetic load in bacterial synthetic biology circuits: convergences with the ohm's law. *Nucleic Acids Res.*, 44(1):496–507, 2015.

[17] Yann Dublanche, Konstantinos Michalodimitrakis, Nico Kümmerer, Mathilde Foglierini, and Luis Serrano. Noise in transcription negative feedback loops: Simulation and experimental analysis. *Mol. Syst. Biol.*, 2:41, 2006.

[18] Irina L Grigorova, Naum J Phleger, Vivek K Mutalik, and Carol A Gross. Insights into transcriptional regulation and $\sigma$ competition from an equilibrium model of RNA polymerase binding to DNA. *Proc. Natl. Acad. Sci. U. S. A.*, 103(14):5332–5337, 2006.

[19] Ron Milo and Rob Phillips. *Cell Biology by the Numbers*. Garland Science, 2015.

[20] H. Bremer, P. Dennis, and M. Ehrenberg. Free RNA polymerase and modeling global transcription in Escherichia coli. *Biochimie*, 85(6):597–609, 2003.

[21] David Kennell and Howard Riezman. Transcription and translation initiation frequencies of the Escherichia coli lac operon. *J. Mol. Biol.*, 114(1):1–21, 1977.

[22] E Schneider, M Blundell, and D Kennell. Translation and mRNA decay. *Mol. Gen. Genet.*, 160(2):121–129, 1978.

[23] Ron Milo, Paul Jorgensen, Uri Moran, Griffin Weber, and Michael Springer. BioNumbers The database of key numbers in molecular and cell biology. *Nucleic Acids Res.*, 38(SUPPL.1):750–753, 2009.

[24] V L Tunitskaya and S N Kochetkov. Structural-functional analysis of bacteriophage T7 RNA polymerase. *Biochemistry (Moscow)*, 67(10):1124–1135, 2002.

[25] Stanley Tabor. Expression using the T7 RNA polymerase/promoter system. *Current Protocols in Molecular Biology*, 11:I:16.2:16.2.1–16.2.11, 2001.

[26] Mofang Liu, Geeta Gupte, Siddhartha Roy, Rajiv P. Bandwar, Smita S. Patel, and Susan Garges. Kinetics of transcription initiation at lacP1. Multiple roles of cyclic AMP receptor protein. *Journal of Biological Chemistry*, 278(41):39755–39761, 2003.

[27] Arbel D. Tadmor and Tsvi Tlusty. A coarse-grained biophysical model of *E. coli* and its application to perturbation of the rRNA operon copy number. *PLoS Comput Biol*, 4(5):1–17, 2008.

[28] Gordon Churchward, Hans Bremer, and RY Young. Transcription in bacteria at different DNA concentrations. *J. Bacteriol.*, 150(2):572–581, 1982.

[29] Jesper Vind, Michael A. Sørensen, Michael D. Rasmussen, and Steen Pedersen. Synthesis of proteins in Escherichia coli is limited by the concentration of free ribosomes: Expression from reporter gene does not always reflect functional mRNA levels. *J. Mol. Biol.*, 231:678–688, 1993.

[30] B. L. Baumgartner, M. R. Bennett, M. Ferry, T. L. Johnson, L. S. Tsimring, and J. Hasty. Antagonistic gene transcripts regulate adaptation to new growth environments. *Proc. Natl. Acad. Sci.*, 108(52):21087–21092, 2011.